

# Between Head and Heart

Exploring interoception on a cortical and subcortical basis

## Master Thesis

Master Cognitive Neuroscience Berlin (MCNB)

Department of Psychology and Education

Freie Universität Berlin

by

**Lisa Sophie Paulsen**

Mat-Nr: 5574504

## Supervisors

Prof. Dr. Huiling Tan

University of Oxford

Prof. Dr. Felix Blankenburg

Freie Universität Berlin

Berlin, 02.12.2025

---

## Master's Thesis Declaration

For the Master's Degree Program in Cognitive Neuroscience at the Department of Education and Psychology, Freie Universität Berlin.

Herewith, I affirm that I wrote the work in hand autonomously and never used another source or resource as declared.



---

Student

Berlin, 02.12.2025

Location, Date

---

## Abstract

Interoception remains an elusive link between the brain and body. While heart–brain coupling has been studied primarily in the context of arousal, its underlying dynamics during rest are still poorly understood but represent a nascent research field. This study examines cortical (EEG) and subcortical, from the subthalamic nucleus (STN) local-field potential (LFP), heart–brain interactions alongside ECG during rest, investigating both the effects of Parkinson drug levodopa and the neural dynamics underlying the heart-evoked potential (HEP). Neural and cardiac activity were recorded from 14 Parkinson’s disease (PD) patients following deep brain stimulation (DBS) surgery under levodopa medication (MedOn, N=14) and, for a subset, without (MedOff, N=8). PD patients were chosen due to the novel possibility of recording intracranial STN LFP after DBS surgery. The presence of levodopa was associated with higher HEP amplitudes in both cortical and subcortical regions, while power, phase, and ECG features showed no distinct medication-related changes. Phase-coherence patterns emerged in inter-trial coherence (ITC) analyses, with significant peaks in the high-delta (2–4 Hz) to low-theta (4–5 Hz) range occurring 100–250 ms after the r-peak. This pattern appeared in both cortical and subcortical recordings and aligns with findings by Park et al. (2018), supporting a phase-resetting mechanism underlying the HEP generation, shaping interoception. The extended delta-range ITC peak suggests a bottom-up contribution of delta activity, consistent with prior evidence linking frontal delta to HEP modulation. The observation that only the HEP differed with medication indicates that levodopa modulates interoception along the central nervous system. In contrast, the impact on interoception through the autonomic nervous system is still elusive. Ultimately, interoception of the heart is dynamically implicated through neural phase in both cortical and subcortical areas.

## Acknowledgements

First and foremost, I want to thank Huiling Tan for her unwavering support and continued guidance. For welcoming me into the lab and creating an inspiring environment to test out ideas and being a part of the research. I want to thank the Tan lab and my office mates, Shenghong He, Alek Pogosyan, Laura Wehmeyer, Sahar Yassine, Fernando Rodriguez Plazas, Jean Debarros, Faissal Sharif, Tao Liu, Xuanjun Guo, Hakimeh Pourakbari, and Benoit Duchet for always being great lunch and discussion partners. You helped me tremendously with your kindness, knowledge, and support. Thank you for making Oxford the place that it is.

Further, I want to thank my home institution, the cognitive neuroscience master's program at the Free University of Berlin, for providing me with resources and the tools to get more in-depth neuroscience knowledge. Special thanks to Felix Blankenburg, Timo Torsten Schmidt, and Ryszard Auksztulewicz for shaping the program.

Lastly, I want to thank my family and friends from all stations of my life for their enduring support and help in making this thesis and shaping me. Especially, Janna, Ana, and Lucy, who have taken the time to review this thesis! Thank you, Max, for always being there.

---

## Table of Contents

<b>1. Introduction.....</b>	<b>6</b>
1.1. Measuring the heart-brain interaction.....	7
1.2. Source Dynamics of the HEP .....	8
1.3. Levodopa influences on the heart .....	11
1.4. Recordings .....	12
1.5. Aim of the project.....	13
<b>2. Methods.....</b>	<b>14</b>
2.1. Patients and surgery .....	14
2.2. Data Recording .....	15
2.3. Study Design.....	16
2.4. Signal preprocessing .....	16
2.4.1. <i>Electrocardiogram (ECG)</i> .....	16
2.4.2. <i>Electroencephalography (EEG) and local field potential (LFP)</i> .....	16
2.5. Analysis and Statistics .....	18
2.5.1. <i>ECG Features Analysis</i> .....	18
2.5.2. <i>HEP Analysis</i> .....	19
2.5.3. <i>ITC Analysis</i> .....	21
2.5.4. <i>PSI/CCC Analysis</i> .....	22
<b>3. Results.....</b>	<b>24</b>
3.1. Levodopa medication showed no effect on ECG features.....	24
3.2. Medication indicates modulation of HEP and phase coherence.....	25
3.3. Delta and Theta phase coherence source of HEP modulation .....	32
<b>4. Discussion.....</b>	<b>35</b>
4.1. HEP driven by phase resetting in delta and theta .....	35
4.2. Levodopa impact on CNS and interoception.....	37
4.3. Phase as a support mechanism for CFA circumvention .....	38
4.4. Limitations and Outlook .....	39
<b>5. References.....</b>	<b>42</b>
<b>6. Appendix.....</b>	<b>50</b>

---

## 1. Introduction

Interoception is responsible for sensing, interpreting, and integrating the body's physiological conditions (e.g., hunger, thirst, pain), thus providing a moment-to-moment map of the body's internal milieu (Berntson & Khalsa, 2021; Craig, 2003). It requires a complex signalling system of the afferent (bottom-up) pathways. A big focus of interoception research has been on cardiac signals as one of the most prominent interoceptive signals. Precise pathways underlying this bottom-up signalling are mostly unknown. Current research has begun to identify several possible physiological pathways between the heart and brain (Critchley & Harrison, 2013; Park & Blanke, 2019; Tallon-Baudry et al., 1996). The well-known pathways starting from the heart are (i) the baroreceptors in the aortic artery travelling via the vagus nerve to the brainstem, (ii) the cardiac neurons in the heart's walls that signal through the vagus nerve or the spinal cord to the brainstem, and (iii) the cutaneous receptors in the skin detecting cardiac changes and transfer them via the spinal cord to the brainstem. From there, they are relayed through the thalamus and terminate at the amygdala (Garfinkel & Critchley, 2016), insula (Strohman et al., 2024), primary somatosensory cortex (Kern et al., 2013) and cingulate cortex (Cambi et al., 2024; for review see Critchley & Harrison, 2013) (**Figure 1**). The connection between interoception and psychomotor processes have implicated the basal ganglia, specifically the neostriatum, in a possible afferent interoceptive pathway (Critchley & Harrison, 2013). Moreover, findings in rodents suggest that cerebral blood pressure changes directly affect local neural activity. One study has seen changes in spontaneous firings after blood pressure alterations in rat slices (Kim et al., 2016). A more recent study in mice found specific baroreceptors in neural populations that open solely to the frequency of the cerebral arteries' blood pressure (Jammal Salameh et al., 2024), thus

indicating that there are increasingly complex mechanisms at work for bottom-up signalling between brain and heart.

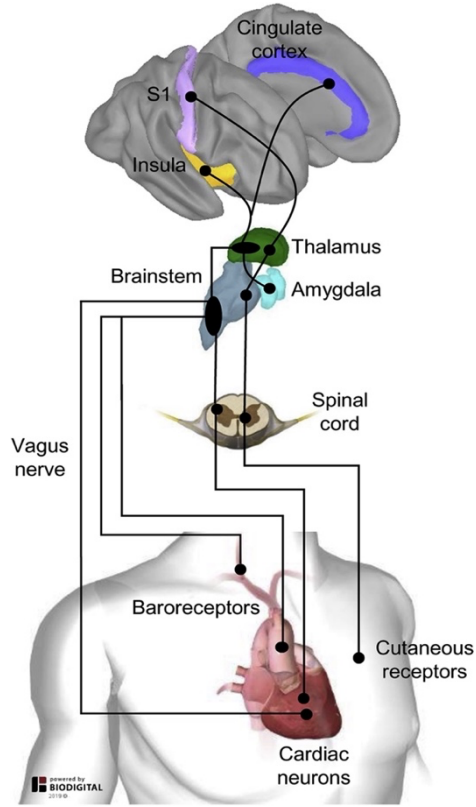


**Figure 1** Possible pathways from the heart to the brain. Cardiac neurons and baroreceptors can signal via the vagus nerve to the brainstem, and baroreceptors and cutaneous receptors can signal via the spinal cord to the brainstem. From there signals are relayed via the thalamus onto the amygdala, insula, primary somatosensory cortex, and the cingulate cortex. Figure from „Heartbeat-evoked cortical responses: Underlying mechanisms, functional roles, and methodological considerations“ by Park et al., 2019, *NeuroImage*, 197, p. 502–511.

## 1.1. Measuring the heart-brain interaction

The increased research interest in cardiac signals has expressed itself in behavioural and physiological measurements to help understand the intricacies of the heart-brain axis as the starting point for interoception. Behaviourally, the heartbeat counting task (Dale & Anderson, 1978; Schandry, 1981), the heartbeat discrimination task (Brener & Ring, 2016; Whitehead et al., 1977), and emotional arousal tasks (e.g. as in Gray et al., 2007; Marshall et al., 2018) have been applied. A key physiological measurement for cardiac signals is heart rate variability (HRV). It reflects the variation in the interval between consecutive heartbeats (Inter-beat Interval, IBI), quantified from r-peak to r-peak measurements in an electrocardiogram

---

(ECG) (Laborde et al., 2017). It has been shown to reflect the dynamic mechanism between the autonomic nervous system (ANS) and cortical interoceptive areas (Garrett et al., 2023). Findings show a positive correlation between interoceptive accuracy and higher HRV, suggesting that the ANS can modulate interoceptive awareness (Lischke et al., 2021; Owens et al., 2018). A meta-study investigating HRV measurements during rest in Parkinson Disease (PD) patients found that parasympathetic (autonomous) cardiac modulation is impaired (Heimrich et al., 2021a), which could influence interoception in PD patients.

Neurophysiologically, the main contender for quantifying interoception is the heartbeat evoked potential (HEP). The HEP consists of electrophysiological data (e.g. electroencephalography (EEG), local field potential (LFP), and intracranial EEG (ECoG)), which is time-locked to the r-peaks of simultaneously measured ECG, proposedly reflecting the cortical processing of cardiac activity (Coll et al., 2021; Park & Blanke, 2019; Schandry, 1981). More recently, a review has connected HEP to interoception across different testing modalities (arousal, interoceptive tasks, and rest) in healthy subjects but also in clinical populations (Coll et al., 2021). HEP recordings are often investigated by comparing groups (Pollatos & Schandry, 2004) or using behavioural tasks (Marshall et al., 2018; Schulz et al., 2015). Resting-state recordings are less prioritised in HEP studies. Most resting state HEP data have been recorded while investigating clinical populations and hypotheses related to the diseases (Müller et al., 2015; Pang et al., 2019; Schulz et al., 2018). Although rest recordings may be especially insightful when looking at the intricacies between HEP and interoception, as they represent the baseline activity of heart and brain coupling.

## 1.2. Source Dynamics of the HEP

Research into the mechanisms and neural sources underlying HEP has only been picked up in recent years (Park & Blanke, 2019). One intracranial ECoG study in epilepsy patients using resting-state data found that changes in HEP, in the time-frequency domain, show no time-locked changes in power but significant changes in phase coherence around 100–250 ms

after the r-peak in 4–7 Hz (theta range) (Park et al., 2018). These findings, employing inter-trial coherence (ITC), led the authors to propose that the underlying mechanisms generating the HEP are not based on amplitude changes time-locked to the heartbeat but on a phase-resetting of the oscillations (Sauseng et al., 2007). The heartbeat resets, as the name suggests, the phase of the oscillations creating a significant phase coherence after the r-peak, which, in an event-related potential analysis, is seen as the HEP. Following the theory of event-related potentials, it is hypothesised that a time-locked event will show an increase in amplitude or power (Park & Blanke, 2019, and Error! Reference source not found.).

Connections between autonomous neural functions and source dynamics in the brain have further implicated delta range oscillations (0.5–4 Hz) to play a pivotal role (Knyazev, 2012). Delta power and oscillations combined with cardiac activity showed a top-down modulation of the HEP in one study (Patron et al., 2019). A causal connection between frontal top-down delta oscillations and interoception was shown in a recent study using transcranial alternating current stimulation, where frontal delta phase synchrony attenuated the HEP. Frontal delta synchrony suppressed interoceptive detection in humans measured by the heartbeat detection task (Haslacher et al., 2025). Moreover, some studies detected a bidirectional coupling of frontal

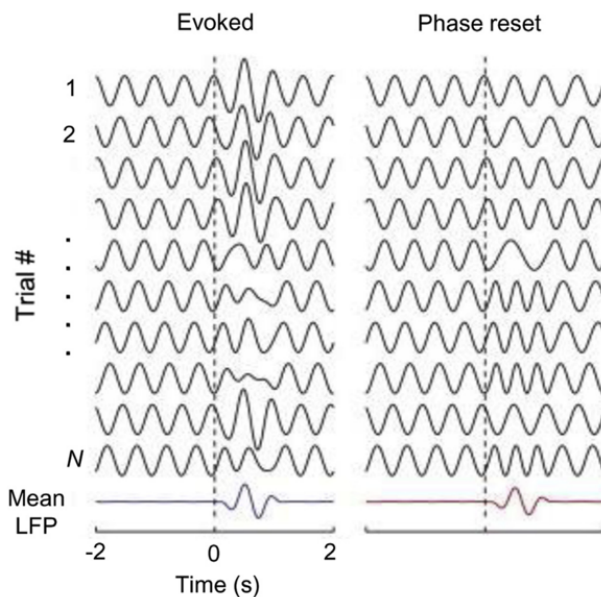


*Figure 2 HEP Source Dynamics Theories.* Visualizing the difference between evoked hypothesis, on the left, and the phase reset theory, on the right. The evoked theory would change the trial based HEP waveform along the amplitude and not phase, as seen after time 0. Where as the phase reset theory shows no changes in the amplitude after 0 but only changes in the phase of the HEP waveforms. Figure from „Heartbeat-evoked cortical responses: Underlying mechanisms, functional roles, and methodological considerations“ by Park et. al., 2019, *NeuroImage*, 197, p. 502–511.

---

delta oscillations and the heartbeat during arousal tasks, finding that bottom-up cardiac activity can influence delta oscillations (Candia-Rivera et al., 2022). However, it remains unclear how delta activity in general could be attenuated by the heartbeat during rest.

Nonetheless, one should be aware that studies investigating HEP face a multitude of challenges. Comparisons between HEP studies are difficult due to low standardisation during preprocessing, choices of HEP epochs, baseline windows and differences in the experimental designs (Coll et al., 2021; Park & Blanke, 2019). Furthermore, in scalp-based recordings time-locked to the r-peak, there remains a visual artefact called the Cardiac Field Artefact (CFA) (Dirlich et al., 1997; Park & Blanke, 2019). It occurs due to the strong electrical field generated by the heart itself. Generally, computational measures were applied to remove the CFA, such as independent component analysis (ICA), the subtraction method, and principal component analysis (PCA). These approaches were effective in removing prominent CFA from the HEP; however, they seem not to extract all artefactual components reliably (Park et al., 2014; Steinfath et al., 2025) and are believed to remove important HEP components (Park & Blanke, 2019). The CFA is thought not to disturb the signal starting from shortly before the t-wave (Dirlich et al., 1997; Gray et al., 2007; Park et al., 2014), creating a way to use non-computational interventions. Conversely, the CFA has only a negligible effect on intracranial recordings and can be disregarded for these measurements (Park & Blanke, 2019). A different artefact comes into play with intracranial recordings, the pulse pressure artefact (PPA), which is based on the electrical signals of the pulse travelling through the cerebral arteries (Kern et al., 2013; Park et al., 2018). No common practice dealing with the PPA has been established yet, since there are currently only a few studies that have investigated HEP using intracranial recordings. One study showed that using time-frequency analysis could be useful for removing PPA, as PPA is characterised by a repetitive oscillatory pattern below 2Hz (Park et al., 2018). The specific frequency range of a subject's PPA can be calculated using their ECG heart rate values. Thus, using a high-pass filter above 2Hz, which is above a healthy human's heartbeat frequency, is thought to suffice in removing the principal influences of the PPA on the HEP in

---

intracranial recording(Kern et al., 2013; Park et al., 2018). However, more research on the PPA and measures to extract it from the data is needed.

### 1.3. Levodopa influences on the heart

Dopamine in the periphery has a known vascular effect, causing vasodilation in low doses and increased blood pressure (BP) in higher dosages (Zeng et al., 2007). Levodopa medication, which is the primary clinical intervention for PD patients, is a precursor of dopamine and norepinephrine. Studies have shown that orally administered levodopa shows a vasodepressor effect in the case of blood pressure (Calne, 1970; Whitsett & Goldberg, 1972). Changes in heartrate (HR) are either reported to be decreased (Bouhaddi et al., 2004; Wolf et al., 2006) or appear unchanged (Calne, 1970; Haapaniemi et al., 2000). Norepinephrine levels show only a slight increase after oral levodopa intake (Calne, 1970). In the past, a decarboxylase inhibitor was added to the levodopa medication, i.e. benserazide or carbidopa (Rinne et al., 1975). These reduce the transformation of levodopa into dopamine in the periphery, decreasing the cardiovascular effects (Noack et al., 2014). Combining BP with ECG recordings during a levodopa challenge with a decarboxylase inhibitor showed that PD patients had a significantly decreased BP but unchanged HR and vasomotor tone after drug intake (Noack et al., 2014). The repeatedly observed levodopa-induced decrease in BP is contrary to the ionotropic effect of peripheral dopamine. The dopaminergic dosage needed to raise the BP via  $\alpha$ - and  $\beta$ -adrenergic receptors is distinctly higher than therapeutic concentrations reached with levodopa medication (Zeng et al., 2007). Studies investigating the BP and HR after levodopa medication without decarboxylase inhibitors did show the same results as studies using decarboxylase inhibitors combined in the levodopa medication (Noack et al., 2014; Whitsett & Goldberg, 1972). Thus, the influence of decarboxylase inhibitor is considered somewhat negligible, and the influence of orally administered levodopa concentration acts contrary to dopamine on the vasocardiac system (Noack et al., 2014). To the best of my knowledge, no further research has been conducted in the field of levodopa influence on the heart-brain axis.

---

## 1.4. Recordings

The main reason for combining local field potentials (LFP) from deep brain stimulation (DBS) electrodes in the subthalamic nucleus (STN) of PD patients and EEG is to understand the dynamics of the HEP in the cortical and subcortical areas. As mentioned above, areas in the subcortex are possibly used for relaying afferent heart signals (thalamus) and as a target region (amygdala). Although of high interest, recordings in subcortical regions in humans are limited to clinical purposes and clinical targets. This is the case because intracranial recordings and surgeries are high-risk and only considered when ethically justifiable and clinically necessary. Thus, the choice of the STN as a recording site for the subcortical measurements is based on clinical interventions. Clinically, it is a highly important implantation site in PD patients as it is related to improved motor function through STN stimulation of the DBS electrodes (Bove et al., 2021; Lachenmayer et al., 2021). Taking into consideration the recent findings of a possible mechanism based on blood pressure through specific baroreceptors in neurons (Jammal Salameh et al., 2024), it can be argued that all areas in the brain receive cardiovascular signals. Given that the precise pathways for the HEP are currently unknown, this implies that not only regions in the proposed pathways might be involved. Furthermore, possible neostriatal projections in the heart-brain pathways implicate the basal ganglia to be included in their dynamics (Critchley & Harrison, 2013). The STN as part of the basal ganglia may suggest that cardiac activity could be recorded from the STN-DBS electrodes. Experimental analysis of the subcortical data of the STN could shed light on the dynamic influence of cardiac signals on areas outside of the possible pathways. Ultimately, the simultaneous recordings of cortical and subcortical electrodes offer the unique possibility of investigating the integration of cortical and subcortical mechanisms underlying the HEP.

## 1.5. Aim of the project

Following the reported literature, this thesis aims to further advance the understanding of the neural source dynamics of HEPs and the influence of levodopa medication on heart-brain coupling. The simultaneous recording of cortical EEG and intracranial subcortical LFP offer a novel opportunity for research into HEPs. HEPs are recorded during eyes-open resting state in both Medication Off (MedOff) and Medication On (MedOn) conditions to assess naturalistic neural processing of the heartbeat, sans behavioural tasks and influences. Medication Off refers to the state of PD patients who have not taken their dopaminergic medication overnight (Mouradian et al., 2025). Based on the literature, I do not expect to see HR, IBI, and HRV-related changes regarding medication, and I expect to see the HEP in both cortical and subcortical data. Starting the exploratory research, I investigate the modulation of the HEP, power, and phase coherence via levodopa. Furthermore, replicating the findings from Park et. al (2018), I envision that after time-frequency analysis, there will be no power changes in the data. However, I expect to find significant phase coherence around the HEP timings in both cortical and subcortical recordings using ITC.

## 2. Methods

### 2.1. Patients and surgery

Fourteen PD patients (seven female, 50%) who underwent bilateral STN-DBS surgery participated in this exploratory study. At the time of the recording, their mean age was 60 years ( $\pm 1.5$  years SEM), with an average disease duration of 11 years ( $\pm 1.6$  years SEM). Participants were recruited from King's College Hospital NHS Foundation Trust and St. George's University Hospital NHS Foundation Trust, both located in London, United Kingdom. All patients gave their written and informed consent to participate in this study. The local ethics committee approved this study (St. George's University Hospital, IRAS: 46576). The patient's clinical details can be found in **Table 1**.

The clinicians used the Medtronic leads (Medtronic Inc., Neurological Division, USA), or the directional leads from Boston Scientific (Boston Scientific, USA) or St. Jude Medical (St. Jude Medical, now Abbott, USA). DBS implantation was guided by magnetic resonance imaging.

Sub.	Gender (f/m)	Age [yr]	Disease duration [yr]	Pre-OP	Pre-OP	Pre-dominant
				UPDSR-III	UPDSR-III	symptoms
				OFF	ON	
1	m	57	11	41	16	Rigidity
2	m	59	6	31	4	Tremor, anxiety with panic attacks
3	f	63	10	29	6	Bradykinesia
4	m	63	20	51	27	Tremor
5	f	62	7	39	5	Tremor
6	f	63	10	29	8	n/a

7	f	64	14	31	17	Tremor
8	f	65	7	23	4	Tremor
9	f	55	8	42	16	n/a
10	f	67	20	55	32	n/a
11	m	50	7	n/a	n/a	Rigidity, bradykinesia
12	m	62	10	n/a	n/a	n/a
13	m	50	7	n/a	n/a	Rigidty and Akinesia
14	f	64	10	n/a	n/a	Balance

**Table 1** Recorded Patients' clinical data. This table shows the PD information from each recorded patient. Pre-OP = pre-operative; UPDSR = Unified Parkinson's Disease Rating Scale.

## 2.2. Data Recording

All 14 patients were recorded once with levodopa medication taken and confirmed to be in effect. For 8 patients, another recording could be done with an overnight withdrawal from levodopa medication. The LFP recordings were completed on externalised DBS electrodes around 2 to 5 days after surgery and before the implantation of the subcutaneous pulse generator. The EEG recordings were split into a main data acquisition phase and a supplemental data acquisition phase. For the main phase, seven electrodes were placed in frontal (F3, F4), central (C3, C4, Cz), and parietal locations (P3, P4, Pz). The main recording included 10 patients. The remaining 4 patients were recorded supplementarily, with differing EEG constellations, due to the different EEG channel requirements of their primary studies. This current study lends itself to easy implementation as only 4 ECG electrodes are added to the setup and resting state data recordings are a foundational part of each study protocol. The exact EEG channels can be found in *Appendix 1*. ECG was recorded using two bipolar electrodes placed horizontally and vertically along the torso around the 4<sup>th</sup> intercostal space. All electrodes used a reference electrode located on the inner wrist of the patients. All signals were measured and amplified (at 2048 Hz) with a TMSi Porti and its respective software (TMS International, Netherlands) on a recording laptop.

## 2.3. Study Design

During the recording, patients were seated comfortably in an armchair. For this thesis, the required data were collected during resting state where patients were asked to sit relaxed with eyes open for about 5 minutes. These 5 minute recordings were conducted with the medication present (MedOn, N=14) and, when possible, again after medication withdrawal (MedOff, N=8).

## 2.4. Signal preprocessing

All signal processing was coded using MATLAB (v. 2024a, Mathworks, Massachusetts, USA) with custom-written scripts. All written code has been made available on the author's GitHub (<https://github.com/lipaulsen/HeadHeart>). The program Spike2 (v. 7.2, Cambridge Electronic Design Limited) was used for the initial visual inspection. R-peak detection in the ECG Signal was performed in Spike2 and manually checked. The data was then visually cleaned by excluding r-peak trials with major artefacts in the EEG and LFP data.

### 2.4.1. Electrocardiogram (ECG)

The ECG data was first cleaned by removing the direct current (DC) offset, and a two-pass 2nd order Butterworth band-pass filter (0.5Hz high pass; 30Hz low pass). The filters used were taken from the fieldtrip toolbox (Oostenveld et al., 2011). Afterwards, the IBI and the HR of each patient were calculated. Using the IBI, the HRV was extracted (**Figure 3B**). These cardiac data features (r-peak, IBI, HR, HRV) were chosen in this exploratory analysis as they represent a broad field of information from the ECG signal.

### 2.4.2. Electroencephalography (EEG) and local field potential (LFP)

The EEG and LFP data were visually inspected using Spike2, and periods with a lot of visual noise were removed. In MATLAB, the data was high- and low-pass filtered using a two-

---

pass 4<sup>th</sup> order Butterworth high-pass filter at 0.5 Hz and the same configuration for the low-pass filter at 100 Hz (**A**).

As mentioned in the introduction, the pulse pressure artefact (PPA) needs to be accounted for in LFP measurements. Another intracranial study used a high-pass filter at 4 Hz for a conservative approach (Park et al., 2018). The mean heart rate (HR) over all patients was 1.28 Hz ( $\pm 0.16$  Hz, min 1.06 Hz, max 1.65 Hz). Based on this, and the fact that pulse-related oscillatory artefacts usually occur below 2 Hz, the more liberal 2 Hz cutoff was chosen for this data to retain the most signal information while still removing the PPA.

Among the methods available for removing the cardiac field artefact (CFA), computational approaches (i.e. ICA, PCA, or subtraction) and non-computational strategies (HEP time window area of interest), the latter was chosen. This decision was based on evidence showing that the CFA amplitude drops to less than 1% during the period from shortly before the t-wave to the subsequent r-peak (Dirlich et al., 1997; Park & Blanke, 2019). Therefore, a restricted timeframe of interest from shortly before the r-wave to the next r-peak was selected, minimizing contamination while maintaining physiological interpretability. This area of interest can be used to measure HEP without CFA contamination and potential signal loss through computational methods.

The EEG and LFP data were re-referenced using the common average reference. Additionally, the LFP data was re-referenced using the bipolar re-referencing method, which is commonly used in LFP data from DBS electrodes (Li et al., 2018). Effectively, this leads to one electrical signal representing the STN per hemisphere. The filtered and re-referenced data was resampled to 300 Hz to speed up the computation. The data was epoched from 300 ms pre to 600 ms post r-peak. Baseline correction was performed using 200 ms of the data from 300 ms to 100 ms before the r-peak of each epoch. Time-frequency decomposition was performed using an IIR Peak Filter with a Bandwidth of 2 Hz and the attenuation QFac of 2Db with 148 frequency bins between 0.5 and 30 Hz, and a resolution of 0.2 Hz. This frequency range was chosen based on previous studies and frequencies of interest including beta frequency (13–30 Hz), since I was

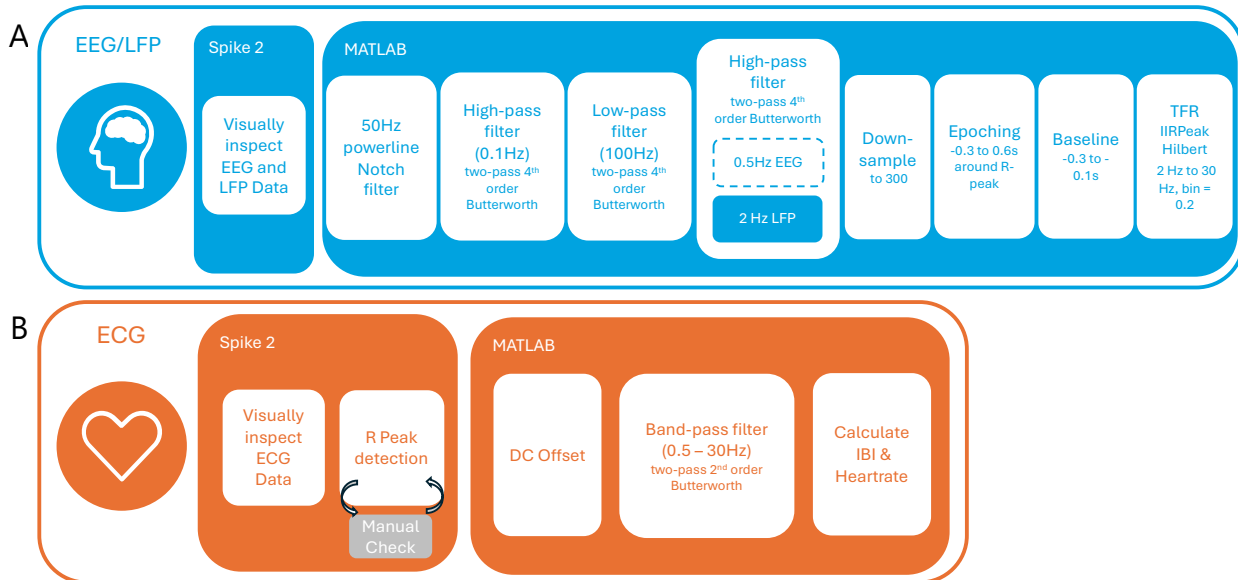


**Figure 3 Preprocessing Pipeline.** (A) The preprocessing for the EEG and LFP starts with visual artefact detection and removal in Spike2. Switching to MATLAB filtering with 50 Hz Notch, a high-pass at 0.1 Hz and a low-pass at 100 Hz was done. An additional high-pass filter at 0.5 Hz for EEG and 2 Hz for LFP was applied to take care of the PPA artefact in the LFP data. The LFP data was bipolar re-referenced, and all data was down-sampled to 300 Hz and epoched time-locked to the r-peak and in the area of interest around -300 ms to 600 ms. All signals were baseline corrected from each epoch the values from -300 ms to -100 ms were subtracted. Ultimately, the data was transformed into the time-frequency domain using the IIRPeak and Hilbert transform. (B) ECG data was visually inspected for artefact rejection, and r-peak detection was automatically done in Spike2 via amplitude thresholding. All detected r-peaks were manually checked. In MATLAB, the DC Offset was calculated, and the data was bandpass filtered at 0.5 to 30 Hz. This led to the calculation of the IBI and the HR through the ECG signal

working with clinical data (Kern et al., 2013; Park et al., 2018). Afterwards, a Hilbert transformation was applied to the filtered data using the respective function from the FieldTrip toolbox. The EEG spectral power and phase time series at each frequency were extracted by computing the magnitude and angle of the Hilbert-transformed signal across time, yielding time-frequency representations of power and phase dynamics.

## 2.5. Analysis and Statistics

All analysis and statistical code can also be found on the author's GitHub (<https://github.com/lipaulsen/HeadHeart>). The significance level for all statistical analyses was set to  $\alpha = .05$ , if not specified otherwise.

### 2.5.1. ECG Features Analysis

ECG data can distinguish multiple features. Features extracted here include the HR, in beats per minute, as r-peaks; the IBI, the time between r-peaks; and the HRV. HRV can be

---

calculated in multiple ways through the ECG signal. The two main approaches discern themselves between frequency-domain or time-domain calculations. HRV not being the focus of analysis, the time-domain calculation Root Mean Sum of Squared Distance (RMSSD) was chosen. It is a widespread and validated approach to HRV calculation that does not use the Fourier transform (Malik, 1996). In this approach, the IBI times are squared, averaged over all values, and ultimately, the square root is taken over the results.

$$\text{RMSSD} = \sqrt{\frac{1}{N-1} \sum_{i=1}^{N-1} (RR_{i+1} - RR_i)^2}$$

RMSSD values are stated in milliseconds and reportedly change over a lifetime. A healthy person aged 30 to 40 years has an RMSSD HRV of 30 to 50 ms, whereas it decreases to roughly 20 to 30 ms for a person in their fifties (Tegegne et al., 2020). Clinical diseases such as PD can influence the HRV. This was shown in a comparison to age-matched healthy controls (Heimrich et al., 2021b). Therefore, it must be considered in the analysis that PD patients' RMSSD HRV values have decreased.

All ECG features are compared between MedOn and MedOff conditions. To inspect the difference in the features between medication, a paired t-test is used. The IBI, HR and HRV values for each patient were averaged and compared between conditions. For only 9 of the 14 patients, both medication condition datasets are available. The other patients opted out of the medication withdrawal, since the increase in PD symptoms during the withdrawal period is too uncomfortable. The data of one of the 9 remaining patients had to be excluded due to arrhythmia leading to the patient's ECG signal being extremely irregular over the entire recording. Thus, the N for the analysis decreased to 8.

### 2.5.2. HEP Analysis

HEPs were computed on the EEG and LFP signals time-locked to the r-peak. R-peak detection was done using Spike2 by automatically tagging each peak exceeding the global

---

average amplitude on a patient-by-patient basis. All automatically tagged instances were visually inspected and corrected. Epochs (-300 to 600 ms regarding the r-peak onset), including excessive artifacts were excluded from the analysis. After artifact rejection, each patient had  $451 \pm 141$  epochs for each electrode. The high inter-patient variability in the number of epochs is due to a few rest recordings only obtaining 3-minute recordings. Then, epochs for each electrode were averaged to calculate the patient's traditional HEP. Subsequently to the traditional averaging, a hierarchical clustering approach was taken to extract waveforms. When plotting the patients' averages of the HEP, it became apparent that the average waveforms of the HEP showed high divergence based on polarity. Hierarchical clustering can alleviate this, as it does not average over the recordings but uses the pure patient-wise waveforms to create clusters over all patients and channels. The average waveform from each channel of each patient was used. A patient and channel-wise waveforms matrix is shaped within a condition over the epoch. Hierarchical clustering is performed using Euclidean distance and the ward algorithm. This creates a hierarchical clustering tree. MATLAB's built-in functions (`cluster`, `pdist`, and `linkage`) were used to compute the hierarchical clustering. A table mapping the patient, channels and clusters was utilised to recover data point assignments. Averaging showed that the shifted polarity of signals led to a loss of useful signals. After inspection, clusters with inverse polarity were flipped to correct for averaging out in this case. Hierarchical clustering was separated into two categories (EEG and STN) based on which channels are clustered, and the two conditions (MedOn and MedOff).

Statistical analysis compared the HEP group waveforms by either medication (MedOn vs. MedOff) or location (EEG vs STN). Statistical significance was determined using a paired t-test with false discovery rate (FDR) correction for multiple comparisons.

---

### 2.5.3. ITC Analysis

To calculate the phase coherence across single trials within one electrode, ITC was used (Tallon-Baudry et al., 1996). It describes the average of normalised instantaneous phases over single trials (Park et al., 2018)

$$ITC(f_0, t) = \frac{1}{N} \left| \sum_{k=1}^N e^{i\varphi_k(f_0, t)} \right|$$

This equation shows the implemented ITC algorithm, where  $f_0$  is the frequency and  $t$  is the time.  $N$  is the number of trials and  $e^{i\varphi_k(f_0, t)}$  converts the phase ( $\varphi_k(f_0, t)$ ) into a complex number on the unit circle using Euler's formula. The resulting values for each trial can range between 0 and 1. A higher value means more coherence during the phase. ITC was calculated for both the EEG and the LFP electrodes for all patients with the above-described epochs.

The statistical analysis was done in reference to the permutation approach from Park et al. (2018) for their ITC analysis. It uses non-parametric permutation statistics with a surrogate (Benjamini & Hochberg, 1995; Maris & Oostenveld, 2007). Surrogate r-peaks for each channel were created by randomly shifting the original r-peak timings 500 ms around the event (-500 ms to 500 ms around the original r-peak). This shuffling period was chosen to conserve the integrity and variability of the original IBI and to keep it within one heartbeat. Using the surrogate r-peaks, the channel data were epoched with these new times and transformed to the time-frequency domain. On the surrogate epochs, the ITC was computed the same way as the original data. The permutation was repeated 1000 times, leading to a distribution of ITC values for each electrode based on chance observation. The z-scores of the distribution were calculated, and p-values for each electrode were extracted.

To replicate the finding of the phase-locking theory, a correlation was calculated between the ITC values and the spectral power during the same epochs. The current data was split into the different EEG recording sites (82 derivations over 14 patients) and LFP (26 derivations over 14 patients). The statistical approach was changed to accommodate the fewer derivations in the

---

present data set. Park et. al. (2018) used a Pearson correlation and z-scored the data within-subject. Compared to the data presented by Park et. al. (2018), the present data set has fewer data points in total and per patient (474 derivations over 8 patients for Park et. al. and 108 derivations over 14 patients in the present data). As the data consists of fewer data points per patient, z-scoring the data would make the correlation unstable due to heteroscedasticity. Thus, the non-parametric Spearman correlation was used for a robust correlation.

Following the previous investigation in the hierarchical clustering, the ITC values were compared between MedOn and MedOff. For each channel all MedOn and MedOff data points were tested using a paired t-test. As in the hierarchical clustering, the issue here remained that MedOff had fewer patients. To maintain a within-subject design, I utilised only patients with MedOn and MedOff data, reducing the N to 8. Beyond that, some patients had a different configuration of EEG channels, as explained in chapter 2.2. Therefore, not all channels have the same degrees of freedom. For multiple comparison correction, FDR was calculated.

#### 2.5.4. PSI/CCC Analysis

Investigating the phase coherence between two electrodes over the trials was done using the Phase Synchronization Index (PSI). In this thesis, it is also referred to as cross-channel coherence (CCC). It calculates the average of the normalised difference of phases over single trials between two channels.

$$\Psi(f, t) = \frac{1}{N} \left| \sum_{k=1}^N e^{i(\varphi_k^{(1)}(f, t) - \varphi_k^{(2)}(f, t))} \right|$$

$\Psi(f, t)$  is the PSI values for frequency  $f$  and time  $t$ .  $N$  is the number of trials with  $\varphi_k^{(1)}(f, t)$  representing the phase angle of signal 1 of trial  $k$  at a certain frequency and time. This is subtracted by the phase angle of signal 2. Using Euler's formula, the complex phase difference is extracted. As with the ITC, the PSI values range between 0 and 1, with higher values indicating higher coherence.

Following the permutation approach from ITC, the CCC analysis also uses surrogate r-peaks to create a range of surrogate epochs. Now two channels are used for this analysis at the same time, and the CCC is calculated in the same way as for the original CCC data. The permutation runs 1000 times, and following that, z-scores and p-values are extracted from the permutation distribution. After inspecting the original and the permutation distribution, it was unequivocal that the permutation CCC distribution differs extensively from the original CCC distribution. Normalisation approaches, like z-scoring to bridge the gap, remained unsuccessful. Other statistical methods, which solely investigate the significant areas of the CCC of parametric tests (i.e., t-test) or non-parametric tests (i.e., Wilcoxon Signed Rank), would test against H0. This course of action does not apply in cases like PSI values, where the range is only between 0 and 1, as the null distribution of the data is not centred around 0. Alas, computational approaches circumventing this issue are out of the scope of this thesis.

Comparing the MedOn to MedOff data of the CCC remained viable. As in the ITC, a paired t-test with FDR was used. The main interest remained in the phase coherence between cortical and subcortical regions. The different CCC configurations were distinguished between ipsilateral and contralateral combinations (**Appendix 2** and **Figure 4**). In the EEG, specific focus was placed on F3, F4, C3, C4, and Pz electrodes. These cover the motor cortex (C3, C4) and frontal regions (F3, F4), which are implicated in motor functions. These areas are further susceptible to the effects of the medication in PD patients.

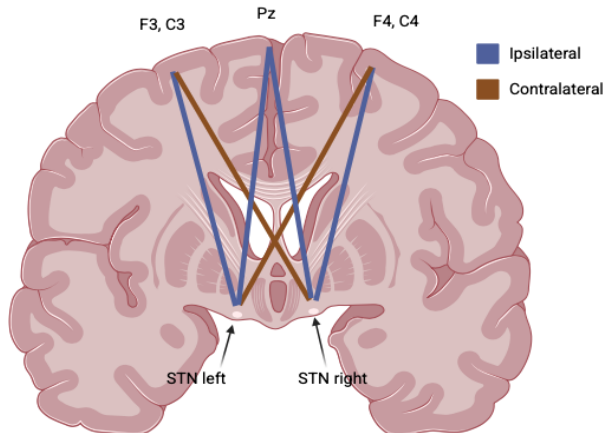


**Figure 4** Visualisation of CCC channel combinations. The shown brain slice is a coronal cut at the level of the basal ganglia. The rough location of the left and right hemisphere STN is indicated, as well as the hemispherical locations of the used electrodes according to the 10-20 placement of EEG electrodes. The colours of the lines indicate whether the combination is considered ipsilateral or contralateral. The graphic was constructed using Biorender.

### 3. Results

#### 3.1. Levodopa medication showed no effect on ECG features

The ECG features, IBI, HR, and HRV were tested, investigating the hypothesis that levodopa medication has an effect on them. Descriptively, median IBI (**Figure 5A**) appeared decreased in MedOn (800 ms) compared to MedOff (900 ms). However, statistically IBI showed no significant difference between medication ( $p = 0.251$ , Cohen's  $d = 0.536$ ). Likewise, median HR (**Figure 5B**) increased slightly in MedOn (75bpm) compared to MedOff (69bpm) showing slower bpm, but no significant effect was found ( $p = 0.338$ ,  $d = 0.454$ ). HRV Analysis (**Figure 5C**) showed no descriptive (median of both conditions = 13 ms) or

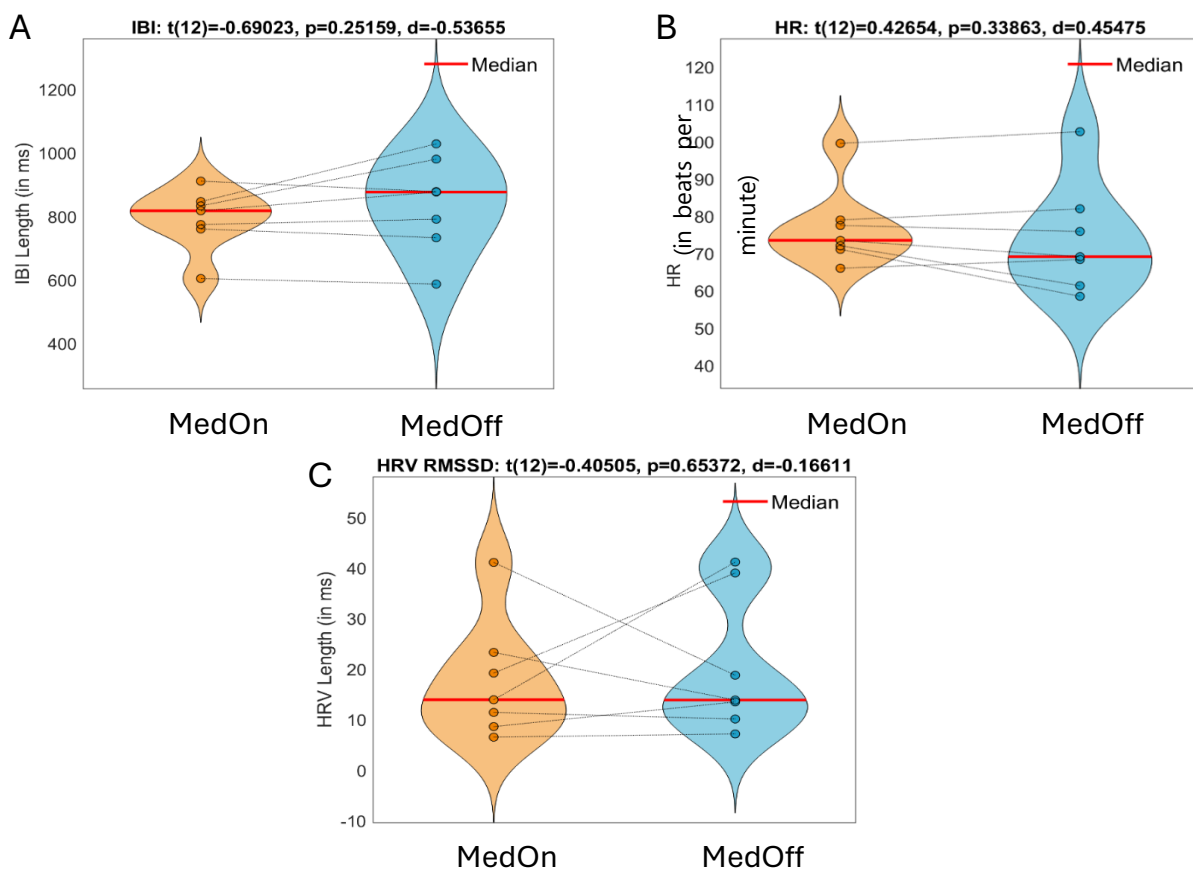


**Figure 5** Statistical Analysis of ECG Features between MedOn and MedOff. All Features are presented using a violin plot showing single data points of the IBI in both medication condition in ms. The red bar shows the median value and the dotted line connecting the conditions indicate the single subject values between conditions. (A) shows the IBI, (B) the HR and (C) the HRV data. Each graph has the mean t-value, df, mean Cohen's d and the p-value threshold in the title.

statistically significant ( $p = 0.653$ ,  $d = 0.166$ ) difference. Single patients presented stark differences in HRV between medication, which does, however, not affect the group analysis.

### 3.2. Medication indicates modulation of HEP and phase coherence

Next, I investigated the medication modulation of the neural data. The HEP averages were calculated for the EEG clusters of frontal (F3, F4), central (C3, C4), and parietal (P3, P4) electrodes as well as for the left (STNl) and right STN (STNr) channels. Descriptively, all EEG clusters showed a slight increase in amplitude around 200 ms after the r-peak (Figure 6A). No

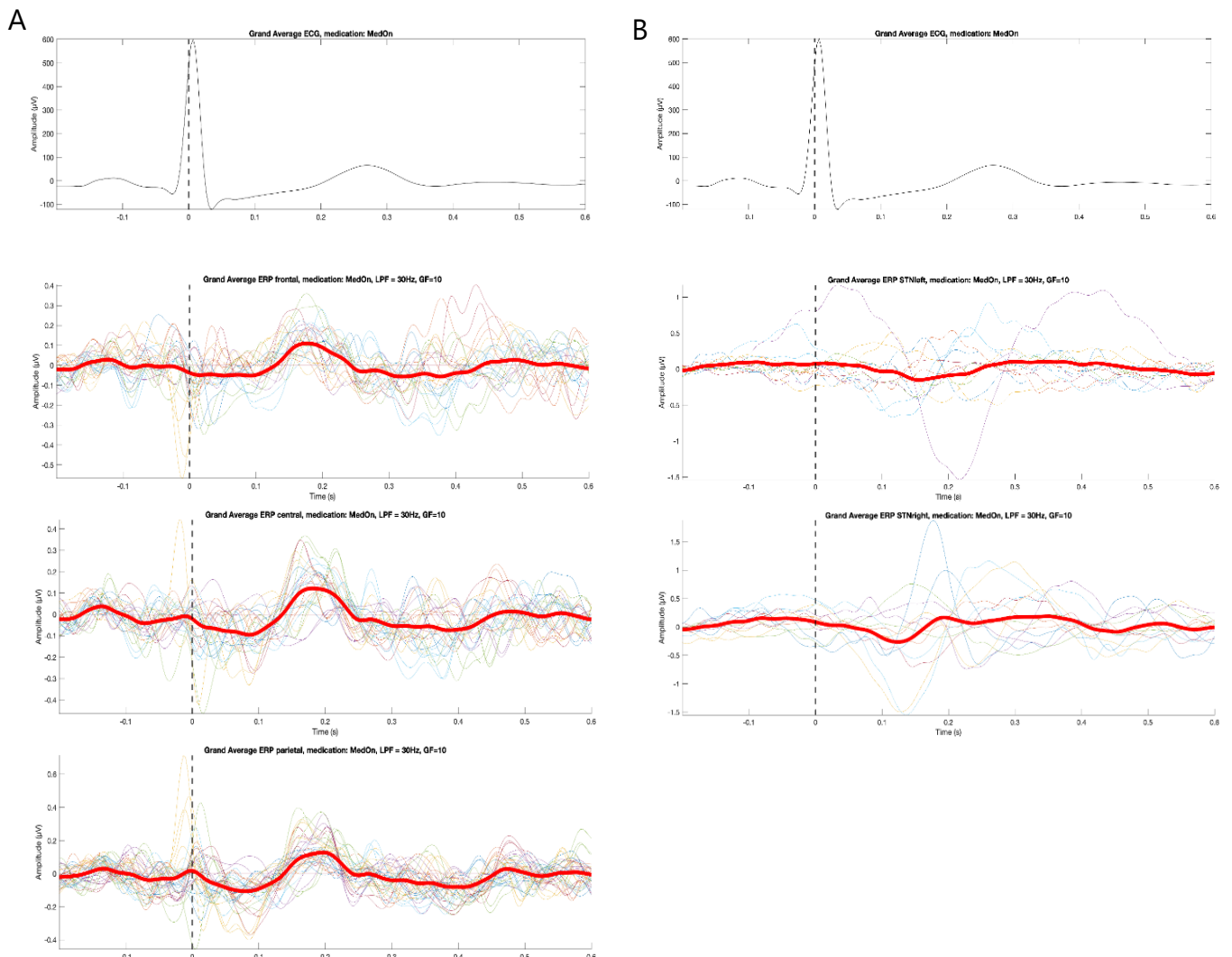


**Figure 6** HEP based on Averaging for EEG frontal, central and parietal regions and STN left and right. In both **A+B** the uppermost graphs show the grand average of the ECG amplitude over time with the black striped line indicated the r-peak. HEP graphs have the r-peak marked with a vertical line. The thick redline represents the grand average of the HEP in amplitude over time. The thin colorful lines represent the single channel HEP within that cluster. All HEPs shown here are MedOn and plotted with a Gaussian filter for smoothing of 10. (**A**) Figures below the ECG show the EEG channel clusters of the frontal, central and parietal electrodes. Average HEP shows only a slight increase in amplitude at the beginning of the t-wave. Single electrode HEPs show a lot of variation. (**B**) No visual amplitude changes in the STNl or STNr HEPs can be observed. Single channel HEPs have a high degree of variance in bipolarity.

---

descriptive changes could be discerned in the STN electrodes (**Figure 6B**). Based on the single-channel HEPs plotted, it could be seen that the HEP has a high degree of variance in polarity around 200 ms after r-peak, which is typically averaged out in the typical HEP calculation. This may explain why there are only subtle amplitude changes in the grand average, prominently prevalent in the case of the STN electrodes. This led me to explore further analysis techniques to fully investigate the HEP.

The initial HEP analysis was extended to hierarchical clustering of the EEG electrodes and the STN electrodes. A paired t-test was conducted to evaluate how medication changes (MedOn vs. MedOff) affect HEP. This procedure tests whether the clustered and bipolarity corrected HEPs change due to medication over time or amplitude. The analysis was conducted with an FDR for multiple corrections implemented after the t-test. None of the significant areas from the t-test survived multiple comparison testing (highlighted areas shown are before multiple comparisons). Be aware that these areas are presented as indicators of a trend in the data, rather than as statistically significant findings. It is revealed that in the EEG electrodes shortly before the t-wave, around 200 ms after the r-peak, HEP with MedOn indicated a dominant increase in amplitude compared to MedOff HEP (**Figure 7A**). Rebound of the MedOn HEP amplitude occurred around 300 ms after r-peak. This appeared steeper than the MedOff rebound which happened at 400 ms after r-peak. During this rebound period MedOff amplitude was higher than MedOn. The rebound, however, was significantly lower in MedOff than in MedOn. Concurrently, in the STN electrodes, the MedOn HEP had a dominantly higher amplitude peak compared to MedOff around 200 ms after r-peak (**Figure 7B**). This peak occurred, as in the EEG electrodes, shortly before the t-wave in the ECG data. The rebound period exhibited the same pattern, with the MedOn HEP showing a steep decline and a comparatively slower decline in the MedOff HEP. Subsequent analysis looked at the comparison of EEG and STN data within either MedOff (**Figure 7C**) or MedOn (**Figure 7D**). No significant amplitude changes occurred within a medication classification. EEG and STN in MedOn had a similar steep rise

and fall of the amplitude peak. Thus, the HEP results suggest a change in medication conditions.

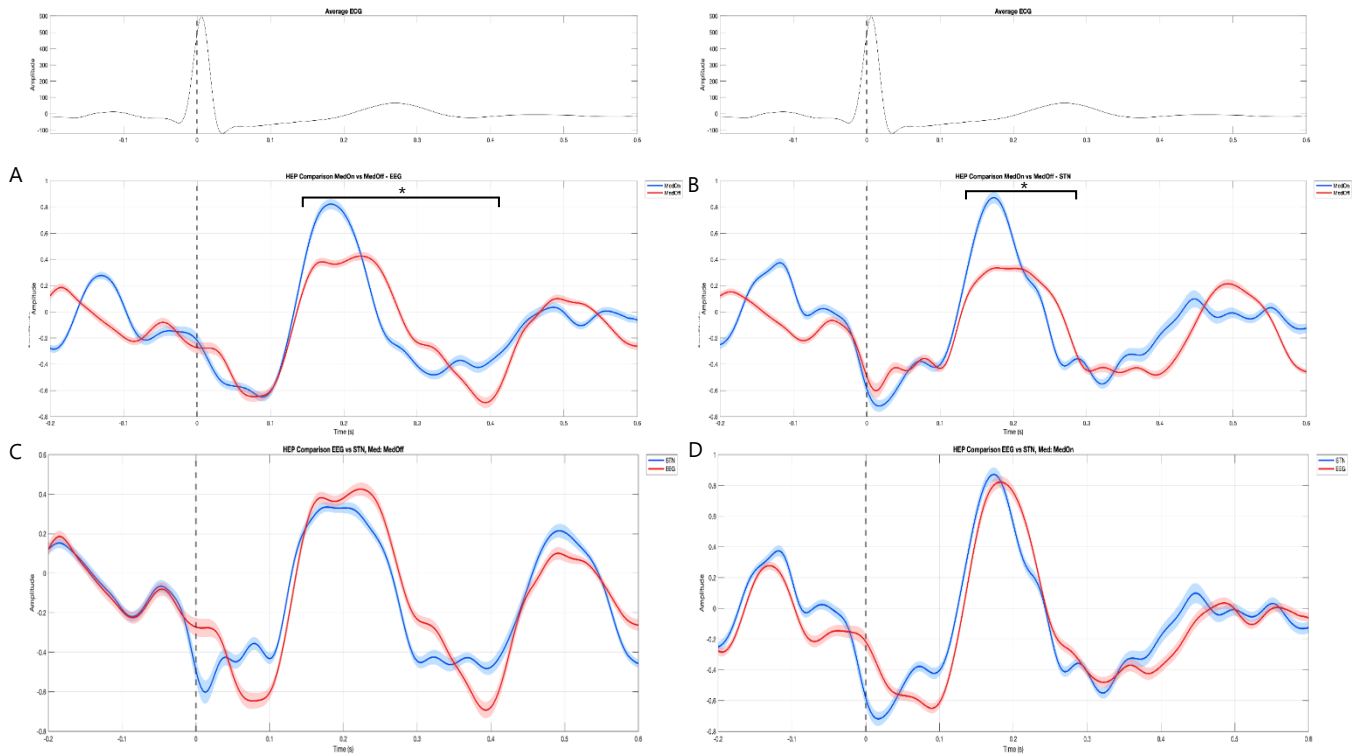


**Figure 7** Hierarchical Clustering EEG and STN MedOn vs. MedOff. Comparison between MedOn and MedOff in either EEG or STN is presented in **A** and **B**. **C** and **D** compare the EEG versus the STN Electrodes in either MedOn or MedOff. Uppermost graphs show the grand average of the ECG amplitude over time, with the black striped line indicating the r-peak. HEP graphs have the r-peak marked with a vertical line. All HEP graphs show the amplitude over time with the shading showing the Mean Standard of Error. Each graphs legend explains the colors of the lines. In **A** and **B** significant areas before Multiple Comparison are marked with a bracket on the top and an asterisk. A paired t-test evaluated statistical significance over time. All significant areas shown in the plot did not survive multiple comparison testing and are only present to show the trend in data.

Power data was extracted through time-frequency decomposition of the signal. Power signals were compared using a paired t-test running over time and frequency. I investigated whether medication changes affected power. As in the previous analysis, a paired t-test was used, where the significant clusters disappeared after multiple comparison correction (MC). Frontal EEG power (**Figure 8A**) indicated a significant increase in MedOff right around the t-wave in the alpha range (mean  $t(7) = 2.602$ , mean Cohen's  $d = 0.9835$ ). Central EEG electrodes (**Figure 8B**) showed separation of medication activation in the frequency range. Power was increased in MedOff in the beta range and in MedOn in the other lower ranges (mean  $t(7) = 3.136$ , mean  $d = 1.185$ ). Indication of significance is mainly spread over the entire time axis, except for alpha range cluster, which only appeared 200 ms after r-peak. MedOff showed stronger power in the beta range in parietal regions (mean  $t(7) = 3.195$ , mean  $d = 1.208$ ) (**Figure 8C**). Fewer

power changes were modulated by medication in the STN electrodes. STN left showed no indication of stronger modulation, but more prevalence for higher power in MedOn (**Figure 8D**). In the right STN, MedOn increased power in a delta-range cluster shortly after r-peak until 400 ms after (mean  $t(8) = 2.792$ , mean  $d = 0.987$ ) (**Figure 8E**).

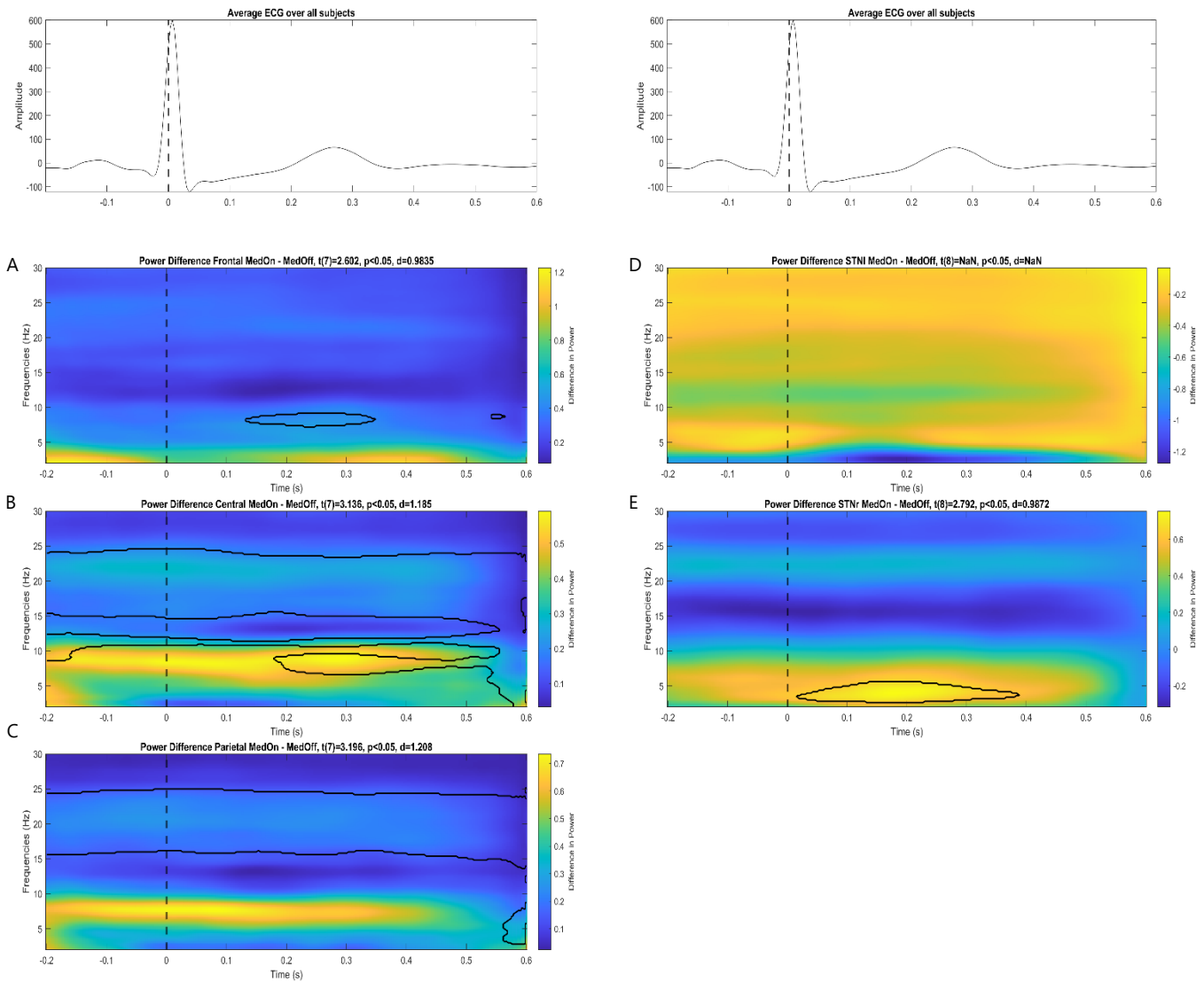


**Figure 8** Time Frequency Power MedOn vs. MedOff in EEG and STN. Uppermost graphs in both columns show the grand average of the ECG amplitude over time, with the black striped line indicating the r-peak. HEP graphs have the r-peak marked with a vertical line. The left column shows the different EEG regions (frontal **A**, central **B**, parietal **C**) and the right STN electrodes. Time frequency plots have the difference of MedOn-MedOff presented with the difference in ITC values. Each graph has the mean t-value, df, mean Cohen's d and the p-value threshold in the title.

I next investigated the effect of medication changes (MedOn and MedOff) on phase coherence using ITC. This was again distinguished between 3 EEG clusters (frontal, central, and parietal) and the two hemispheric STN channels. A paired t-test was calculated over time and frequency levels of the ITC values. In **Figure 9** the time-frequency plots show black rimmed clusters.

Those indicate significant areas before multiple comparison (MC), as none of these clusters survived that line of testing. As in the previous plot, the pre-MC significant clusters were solely used as indicators of a trend. Frontal EEG electrodes (**Figure 9A**) showed mainly a higher phase coherence in MedOff right around r-peak in high beta (21–30 Hz). This switched to a slightly higher high-beta ITC value in MedOn around 550 ms after r-peak. Lower frequency (delta, theta) areas showed a higher ITC in MedOn shortly before t-wave. This pattern continued over the central and parietal electrodes (**Figure 9B-C**), with higher MedOff ITC values in the beta frequency especially around or shortly after r-peak. The lower frequency ranges presented increased ITC values in the MedOn condition. Switching to LFP, the left STN channel showed

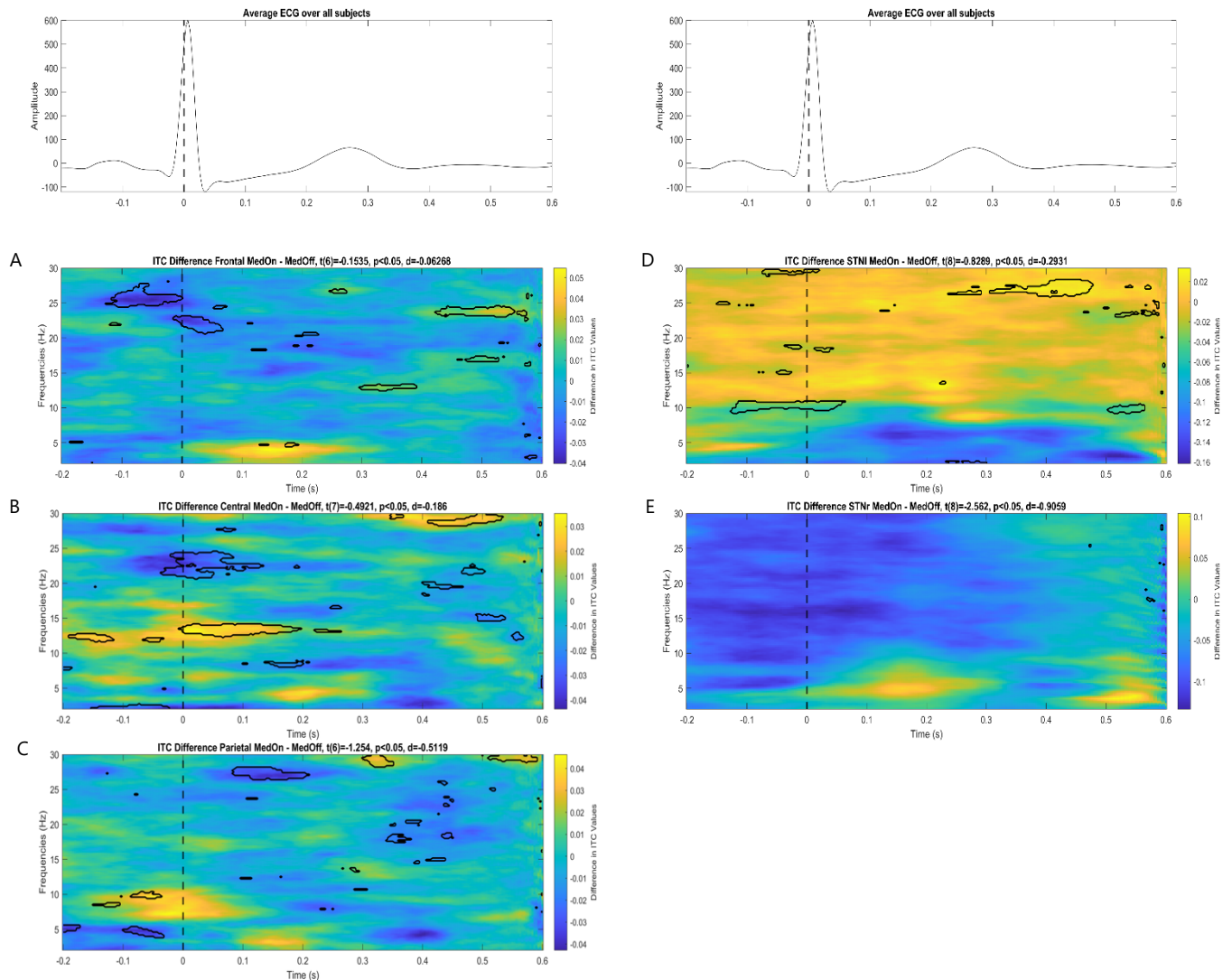


**Figure 9:** Effect of medication on ITC values in EEG and STN. Uppermost graphs in both columns show the grand average of the ECG amplitude over time, with the black striped line indicating the r-peak. time-frequency graphs have the r-peak marked with a vertical line. The left column shows the different EEG regions (frontal **A**, central **B**, parietal **C**) and the right STN electrodes. Time frequency plots have the difference of MedOn-MedOff presented with the Difference in ITC values. Each graph has the mean t-value, df, mean Cohen's d and the p-value threshold in the title.

a trend towards higher ITC in MedOn, contrary to the just presented EEG results. Right STN remained mainly without clear indicators of significance. Higher ITC in MedOn was present at 150 ms and 550 ms after r-peak in the delta/theta range, the rest remaining higher ITC MedOff values.

Furthermore, I explored the modulation of medication on ipsilateral and contralateral phase coherence between the subcortical STN and the cortical EEG electrodes. The channels investigated are STNI-F3, STNI-C3, STNI-Pz, STNr-F4, STNr-C4, on the ipsilateral side and STNr-Pz. For the contralateral connection, the frontal and central hemispheric channels are switched, resulting in STNI-F4, STNI-C4, STNr-F3, and STNr-C3. Significant areas after the paired t-test did not hold up to MC but are used as an indication guide. The most prominent features for both the frontal electrodes ipsilateral to the STN electrodes were that the phase coherence was stronger in MedOff, specifically in the low beta range (mean  $t(7) = -2.42$ , mean

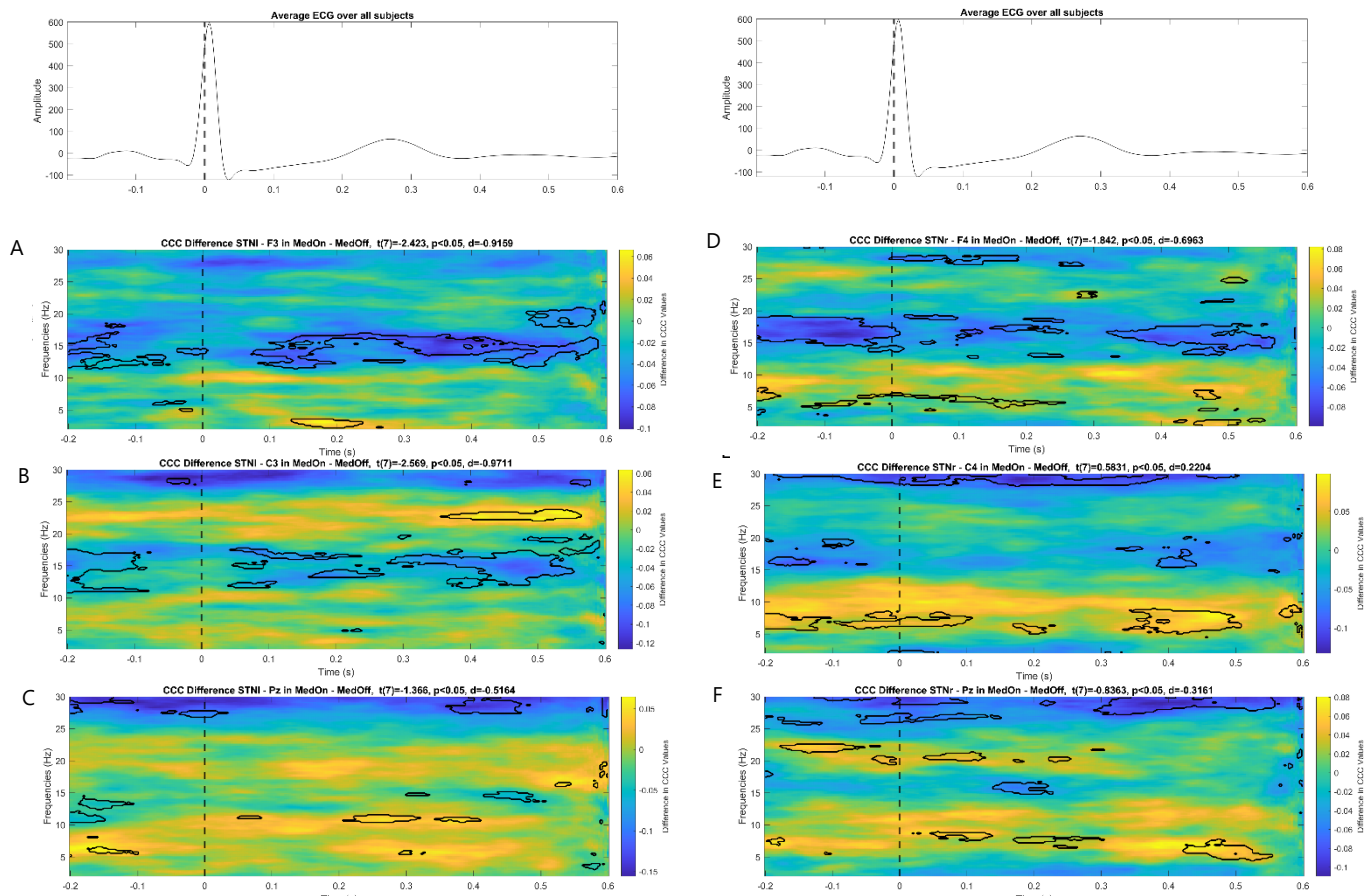


**Figure 10** *Ipsilateral phase coherence between EEG and STN electrodes* Uppermost graphs in both columns show the grand average of the ECG amplitude over time, with the black striped line indicating the r-peak. Time-frequency graphs have the r-peak marked with a vertical line. The left column shows the different EEG regions (frontal **A**, central **B**, parietal **C**) and the right column shows STN electrodes. Time-frequency plots display the difference between MedOn and MedOff, along with the Difference in CCC values. Each graph has the mean t-value, df, mean Cohen's d and the p-value threshold in the title.

$d = -0.915$ ) (**Figure 10A+D**). The frontal electrodes presented randomised clusters of higher MedOn phase coherence in the lower frequency ranges. The ipsilateral central EEG electrodes exhibited diverging results compared to the parallels the frontal electrodes. STNl-C3 continued with the higher low beta coherence over the entire time-axis (**Figure 10B**). Surprisingly, CCC in high beta in the later part of the cardiac cycle showed higher MedOn phase coherence. No discernible mentions could be made about the lower frequency ranges, whereas the right hemisphere STNr-C4 displayed a stronger prevalence for MedOn phase coherence across cortical and subcortical areas, especially in the lower frequency ranges (theta and alpha) (**Figure 10E**). Ipsilateral phase interaction between the subcortical regions with Pz proved to be random, with no perceivable patterns (**Figure 10C+E**).

Looking at the contralateral hemispheres between subcortical and cortical areas I discovered that the left STN electrode showed no detectable separation in clusters between time, frequency and medication change (**Figure 11A+B**). Right STN presented with a more separated coherence profile (**Figure 11C+D**). High beta area was mainly modulated by the absence of medication regardless of time. Contrary to this, the theta and alpha areas' phase coherence seemed to be driven by the presence of medication.

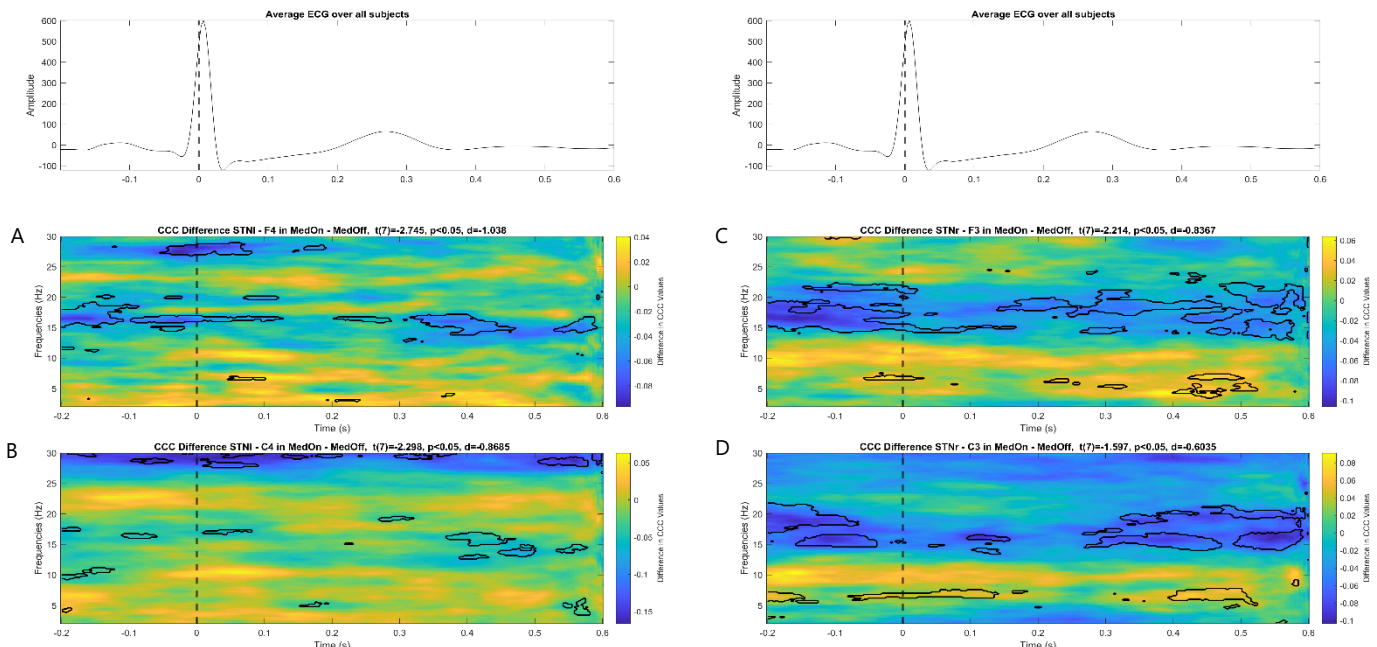


**Figure 11** Contralateral phase coherence between EEG and STN electrodes. Uppermost graphs in both columns show the grand average of the ECG amplitude over time, with the black striped line indicating the r-peak. Time-frequency graphs have the r-peak marked with a vertical line. The left column shows the different EEG regions (frontal **A**, central **B**, parietal **C**) and the right column shows the STN electrodes. Time frequency plots have the difference of MedOn-MedOff presented with the difference in CCC values. Each graph has the mean t-value, df, mean Cohen's d and the p-value threshold in the title.

---

### 3.3. Delta and Theta phase coherence source of HEP modulation

I next investigated the neural sources underlying HEP, following the example of Park et al. (2018). The data differentiation used offers a broader insight into the neural sources in subcortical regions as well. Grand-averaged ITC was calculated for the frontal, central and parietal EEG clusters, as well as for both hemispheres of STN electrodes. The current analysis does not depend on the comparison of MedOn and MedOff, thus, to broaden the statistical power, solely MedOn data was used to increase the sample size to 14 patients. This exploration helped determine the frequency time phase coherence during the HEP. Over all electrodes I found that ITC significantly increased after r-peak (**Figure 12**, using surrogate permutation statistics with  $p < 0.005$ ). The strongest phase coherence in the EEG was found around 100 to 250 ms after r-peak (**Figure 12A-C**, peaks are highlighted within the white boxes), which temporally aligns with the ECoG findings from Park et. al. (2018). This period was expanded in the STN electrodes to the strongest ITC period, ranging from 100 to 300 ms after r-peak (**Figure 12D+E**). Contrary to the Park et. al. (2018), I included the high delta range (2–4 Hz) within my analysis, with a low pass filter of 2 Hz instead of 4Hz. Including delta showed that the strongest ITC enhancement was in the delta range (2–4Hz) and low theta range (4–5Hz). This is the case for both EEG and STN data. Additionally, in the EEG electrodes, a significant area right around the r-peak ( $\pm 100$  ms) was present, which stretches across the entire frequency band. This pattern is absent in the STN electrodes.

The relationship between power and HEP has been shown multiple times in the past. I could already see in the MedOn MedOff difference that there are no time-specific power changes. Purely looking at the power revealed that there is no time-locked change to the r-peak (**Figure 13A-E**). To validate the power analysis, I checked whether the power would show HEP-unrelated continuous PD-specific beta power increase. **Figure 8C+D** visually showed that power in beta is higher during MedOff than MedOn. This follows the common knowledge that beta power is increased in PD patients. Extracting the beta range of the power reveals that beta

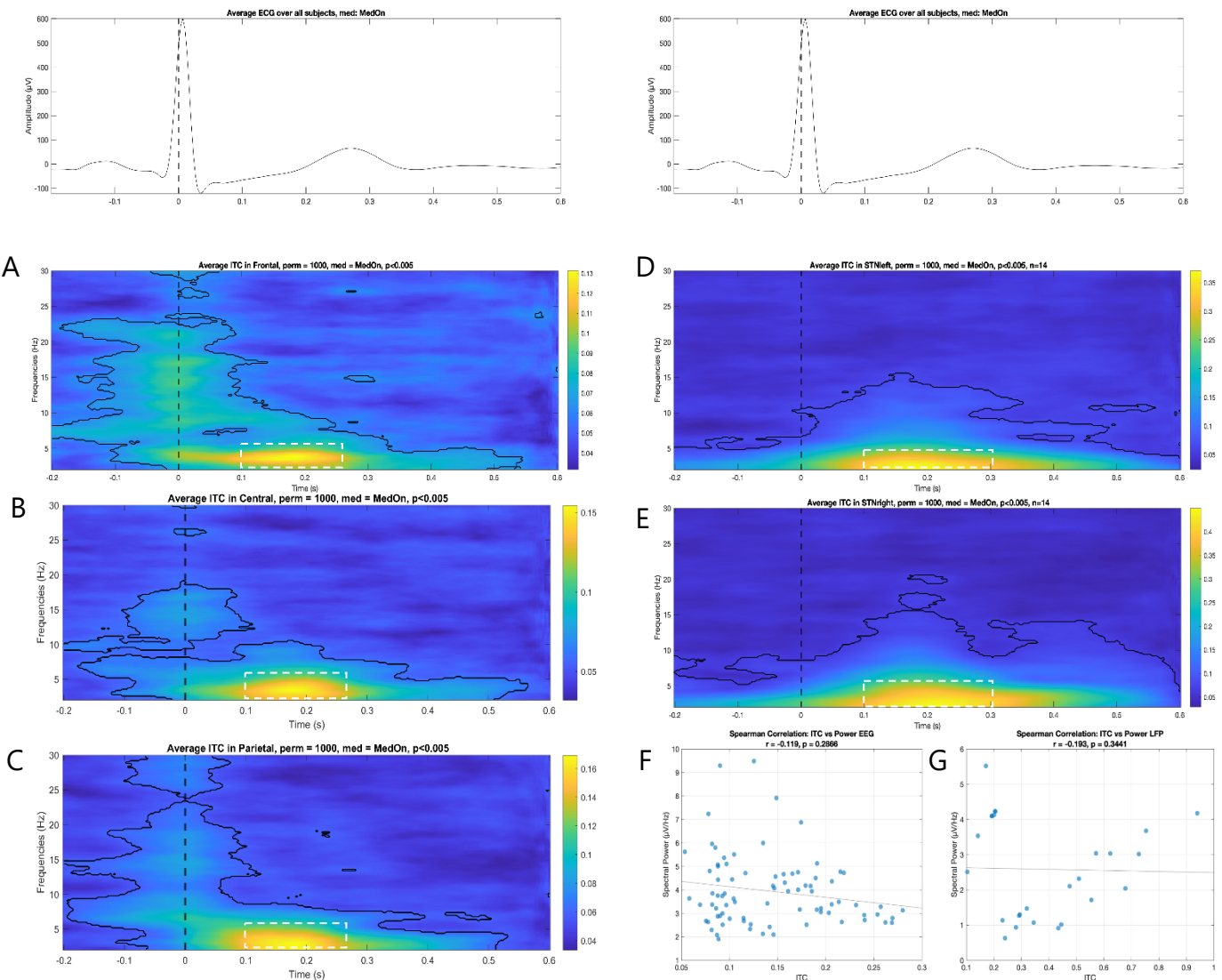


**Figure 12 ITC across EEG and STN and correlation.** Uppermost graphs in both columns show the grand average of the ECG amplitude over time, with the black striped line indicating the r-peak. Time-frequency graphs have the r-peak marked with a vertical line. The figure shows the different EEG regions (frontal **A**, central **B**, parietal **C**) and the STN electrodes (STNleft **D**, STNright **E**). The black outline in those graphs shows significant areas after surrogate permutation statistics using 1000 permutations and a  $p < 0.005$ . The white dashed box shows the ITC Peak area within the significant area. Using the mean of the ITC peak area, it was correlated with the mean power in the same area. **F** shows that there is no significant correlation between mean ITC peak values and spectral power in the EEG electrodes. The same thing was correlated for the STN electrodes, showing no significant correlation. **R** and **p** values are presented on top of the correlation plots.

power remains high (**Figure 13F+G**). Generally, EEG and STN electrodes have no visual or statistical significant change in power over all frequency bands (**Figure 13A-E**). Thus, my power analysis reliably showed no effect to HEP. Testing for the relationship between power and phase of the HEP, I conducted a correlation. This analysis, inspired by Park et al. (2018), took the mean ITC and mean power within the significant peak cluster. The specific statistical procedure and modifications based on my data is explained in chapter 2.5.3. For both EEG and STN, Spearman's  $r$  revealed no significant correlation between ITC and power (**Figure 12F+G**). Ultimately, presenting that phase coherence in delta and theta modulates HEP, power shows no association with HEPs, and no correlational relationship exists between power and phase in HEP.

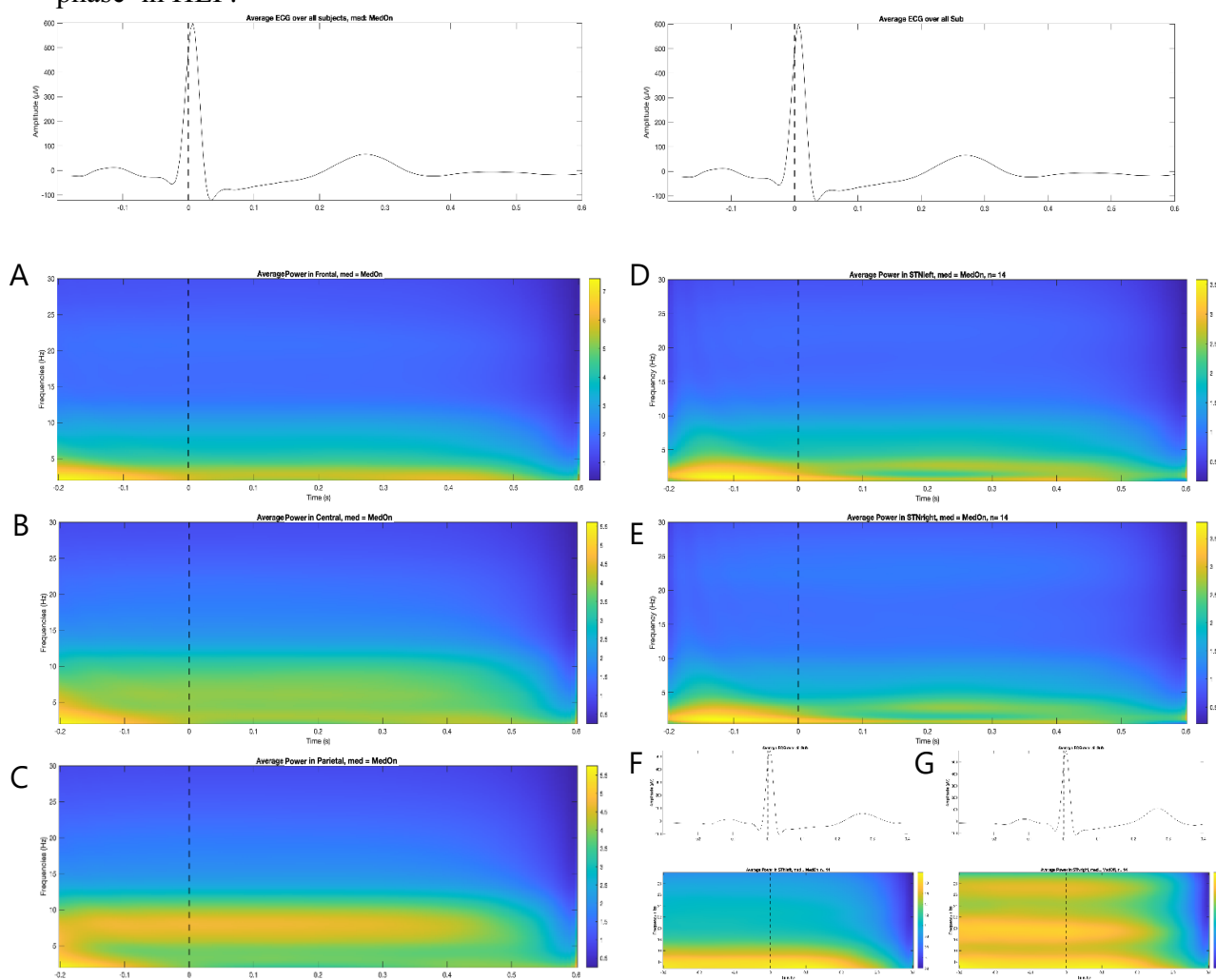


**Figure 13** Power in the cardiac cycle of EEG and STN. Uppermost graphs in both columns show the grand average of the ECG amplitude over time, with the black striped line indicating the r-peak. Time-frequency graphs have the r-peak marked with a vertical line. The figure shows the different EEG regions (frontal **A**, central **B**, parietal **C**) and the STN electrodes (STNleft **D**, STNright **E**). **F+G** show the spectral power in just beta range of the STNleft and STNright.

---

## 4. Discussion

Cortical and subcortical data from 14 patients with Parkinson's disease were collected, and found that delta and theta range phase coherence underlie the source dynamics of HEP. Mean ITC peak data was correlated with the power spectra data of the same area and revealed no correlation of ITC peaks with power, stating that significant ITC was irrespective of power. Moreover, the data indicated that the presence of dopaminergic medication in PD patients influenced interoceptive bottom-up signalling in the brain. Various analyses compared medication, showing a discernible difference in HEP. Conversely, the investigated ECG features showed no effect by medication. This is in line with the divergence in findings of the levodopa research using ECG, which either found no or subtle changes (Bouhaddi et al., 2004; Calne, 1970; Haapaniemi et al., 2000; Wolf et al., 2006). The present data suggests that dopamine influences the specific HEP pattern by increasing HEP amplitude and shortening the length of the HEP peak. Finally, the ITC EEG results show a specific pattern which does not occur in the ITC STN, suggesting that CFA could be observable using ITC, opening further research for an advancement into CFA's possible methodical approaches for artefact removal. To the best of my knowledge, this is the first study investigating heart-brain interoception on a subcortical and cortical basis during rest. It showed that phase specifically modulates HEP and that phase analysis opens new avenues for this line of research.

### 4.1. HEP driven by phase resetting in delta and theta

The ITC and power analysis of the HEP in the time-frequency domain support the phase-resetting hypothesis that Park et al. (2018) supposes. After replicating their analysis, I could find high phase coherence in the same time range. This is coupled with the finding that there is no correlation between ITC peak and the spectral power, which Park et al. (2018) also found. This mechanism of the source dynamics shows no power change time-locked to the r-peak in the HEP, underlined by significant phase coherence. The evoked model (Park & Blanke, 2019

---

and Error! Reference source not found.) would propose a time-locked change in power. An observed difference is the frequency range implicated in the ITC peak; Park et al. (2018) found the theta range (4–7 Hz) to be crucial. In the present data, I found values in the high delta (2–4 Hz) and low theta range (4–5 Hz). High theta shows significant phase coherence but outside of the realm of the ITC peak. Park et al. (2018) eradicated delta signals due to high-pass filtering at 4 Hz, as a more conservative approach to circumvent PPA.

I showed that in both subcortical and cortical findings, delta phase coherence peaks between 150–300 ms after r-peak and modulate the HEP during rest. Previously, heartbeat-attenuated delta findings have been observed primarily in spectral power in the frontal area during arousal tasks. Delta phase has been implicated in the top-down attenuation of the HEP. Research and implications of delta in bottom-up interoception beyond a bi-directional influence have not been seen (Candia-Rivera et al., 2022). Thus, the present resting data expands the realm of delta involvement complementary to top-down interoception to include bottom-up interoception. This implies that the underlying patterns in creating the HEP expand beyond theta. Theta band has been shown in vagus nerve modulation to influence the bottom-up creation of HEP, which supports the influence of theta's involvement in interoception beyond my findings (Poppa et al., 2022). One consideration in the interpretation of the results regarding delta remains that delta range activity and phase can be dysfunctional in patients with brain damage (Assenza & Di Lazzaro, 2015). As PD patients are recorded who have received DBS, which is solely considered in a medium to late progression of the disease with symptomatic damage to the basal ganglia, delta range activity might be abnormal compared with to healthy controls. One study found that ITC values of delta and theta were decreased in PD patients compared to healthy controls (Hünerli-Gündüz et al., 2023). Further testing with age-matched controls to verify delta's influence is necessary. Ultimately, the presented ITC findings might be less prominent compared to a healthy population, but they remain significant. This indicates the strength of the ITC peak in delta and theta in underlying HEP generation via phase resetting. I showed that the timing of the ITC peak in the cortical and subcortical areas occurs 100–300

---

ms after r-peak, supporting the hypothesis that phase resetting underlies HEP generation. Further supporting this is the finding that the peak HEP timing from my hierarchical clustering temporally overlaps with the peak ITC timing. Ultimately, I would propose that delta phase resetting, in addition to theta phase resetting, may be involved in the generation of the HEP, although further studies are needed to confirm this.

## 4.2. Levodopa impact on CNS and interoception

The presented findings suggest that there is a modulation in neural signalling during the cardiac cycle through levodopa medication. ECG features show no effect from medication as could be expected from previous literature (Calne, 1970; Haapaniemi et al., 2000). Especially HEP waveforms using the hierarchical clustering method indicated an impact on interoception processing due to the presence of medication. Further time-frequency analysis (power, ITC, CCC) showed no clear differentiations or patterns that could be used to interpret medication influence. Contrary to my findings, other studies have seen a significant increase in HRV, based on a single dose of levodopa compared to MedOff in PD patients (Meng et al., 2015). Specific medication details, such as medication type and dosage, are not available for my dataset. So further analysis based on those factors could be a focus for future research. To the best of my knowledge, the effects of levodopa medication on HEP had not been investigated before. Therefore, it is a revelation that my data indicates that neural waveforms showed an increase and sharpness in amplitude in the HEP due to the presence of levodopa. These changes in the HEP would suggest that levodopa had a modulating effect on interoception within the central nervous system (CNS). The data cannot shed light on levodopa's effect on the ANS, as previously seen, levodopa's main effect is hypotensive (Calne, 1970; Noack et al., 2014; Whitsett & Goldberg, 1972). Since this study had no BP measurement during the data acquisition, a full interpretation on the mechanisms in the ANS due to levodopa medication could not be done. Investigating the complex mechanisms dopamine has on the brain, coupled with interoception, can help in medication adjustments. Furthermore, it might help understand

---

the connection between interoception and the dopamine network by uncovering how the presence of dopamine in the brain might influence bottom-up signalling from the body. This could be enlightening in the case of diagnoses related to dopamine dysregulation conditions, including but not limited to PD, attention deficit and hyperactivity disorder, schizophrenia or addiction.

#### 4.3. Phase as a support mechanism for CFA circumvention

The reported ITC findings include another revelation. In the EEG trial-based ITC, I could observe, besides the delta-theta peak, a whole frequency band spanning phase coherence  $\pm 100$  ms around the r-peak. This pattern was only present in the EEG electrodes and was completely missing in the LFP electrodes. A difference in the analysis of heartbeat-locked EEG and LFP data is the presence of the CFA which, as previously discussed, solely occurs in EEG data as CFA influence in intracranial recordings is negligible (Park & Blanke, 2019). One big issue in the pre-processing of data investigating HEP is the artefact removal of the CFA, as there are no distinct and reliable measures. Previous studies have indicated time periods in which the CFA amplitude drops to less than 1% during the range of interest (Dirlich et al., 1997; Park & Blanke, 2019), but these time periods have differed greatly between studies. Within rest recordings in clinical populations, the main HEP timings were either between 200–300 ms or between 400–500 ms after r-peak (Coll et al., 2021). As a non-computational approach was chosen, the phase coherence pattern right around the r-peak, which is purely present in the EEG data, could be a strong indicator for the CFA. This revelation comes due to the novel quality of having both cortical and subcortical data, and thus being able to compare the ITC values of EEG and STN. In the presented data, I can see that the frequency band spanning significant ITC values right around r-peak are in the time frame between 100 ms before to 100 ms after r-peak, using the baseline window of 300 to 100 ms before the r-peak of each trial. This recognisable pattern cannot be seen in the power spectral analysis or in the HEP, which underlines the difficulty in pinning down specific CFA quantification. As a methodological

analysis is out of the scope of this thesis, no foundational analysis can be provided. Moreover, I would like to propose this finding as a starting point for further analysis into this phenomenon, which overlaps with what the research would imply the features of CFA to be. Ultimately, this could aid the future of a comprehensive and established pre-processing in the analysis of interoceptive heart-brain coupling research.

#### 4.4. Limitations and Outlook

The study design follows the exploration of the data. This can harbour many advantages for curiosity but conversely provides limitations. Conceptually, the requirements for data acquisition are low, with resting state recordings of 5 min and 2 extra bipolar ECG electrodes added onto an already used EEG amplifier for electrophysiological recordings. It can very easily be implemented into other EEG studies. A pitfall in the presented data is the different combinations of EEG electrodes. Some electrodes might only have an N of 1 or 2, so a more consistent and stable set of electrode parameters would alleviate analysis issues. Moreover, this study only had a subset of patients in both conditions (MedOn and MedOff). For further studies, I would aim to have a reliable condition split for increased statistical reliability. Following this, the study's main drawback for most statistical tests was its low sample size, which inadvertently decreased statistical power. Thus, all the comparisons for medication are not statistically significant after multiple comparisons. Investigating the influence of medication on neural responses of interception with a high sample size would improve statistical analysis. As discussed previously, investigating time-locked heart and brain data leads to artefact management in the cortical region with CFA and in the subcortical region with the PPA. Currently, there is no common ground for a procedure to deal with either artefact in the different modalities of EEG and LFP, leading researchers to possibly under- or overcorrect during artefact removal, influencing results. This lack of shared pre-processing practice has been noted before. Park and Blanke (2019) have suggested a pre-processing procedure. Only a

---

few papers reported knowledge of, or performed this procedure. For future research, an updated approach, taking current developments into account, would be commendable.

Finally, clinical research with an older population with previous conditions can also include heart conditions apart from the PD diagnosis. In the presented study, patients were included based on the DBS surgery and PD diagnosis, and other heart diagnoses were not regarded. Controlling for heart conditions or heart medications, previous to recordings, could help with exclusion criteria.

Furthermore, the exact medication and dosage of levodopa were not recorded for each participant. This limits the interpretation of the medication influence. Henceforth, it would be advisable to record dopaminergic medication to control for levodopa influence, including the decarboxylase inhibitor. However, on a cardiovascular basis, levodopa medication, including and excluding decarboxylase inhibitor, have shown no significant cardiovascular effects in peripheral measurements (Noack et al., 2014; Whitsett & Goldberg, 1972). The influence of the levodopa in the periphery and its subsequent effect on HEP has not been controlled for yet. This study utilised solely electrophysiological measurements, but an additional BP method would be beneficial to control for levodopa changes and to open up the investigation in blood pressure-guided changes in the brain as seen in mouse models (Jammal Salameh et al., 2024; Kim et al., 2016).

#### 4.5. Conclusion

The presented study provides evidence that heart-brain interoception can be examined simultaneously at cortical and subcortical levels during rest, revealing source dynamic insights into the generation of the HEP. The findings demonstrate that HEPs in patients with PD are primarily based on phase resetting in the delta and theta range, rather than by changes in spectral power, supporting the phase-resetting theory. Importantly, phase coherence peaked 100-300 ms after the R-peak in both EEG and STN recordings, underscoring a temporal dynamic underlying HEP generation. Dopaminergic medication was found to modulate

---

interoceptive processing in the CNS, increasing and sharpening HEP amplitude, while leaving ECG features unchanged. This suggests that dopamine specifically influences neural, but not peripheral, components of interoception, showing a modulation between levodopa and heartbeat-related cortical processing worthy of further investigation. Additionally, the comparison of cortical and subcortical phase coherence revealed a distinct ITC pattern only in the EEG electrodes surrounding the R-peak. This pattern aligns with characteristics of the CFA. This novel observation suggests that phase-based measures may offer a promising avenue for future CFA characterisation and artefact removal strategies. Despite limitations such as a modest sample size, heterogeneous EEG electrodes, and limited medication and previous cardiac disease information, the results establish interesting findings for future HEP and interoception research. Overall, this work shows that phase dynamics provide insight into the mechanisms of interoception, emphasising the relevance of delta and theta rhythms, dopaminergic modulation, and methodological innovation in advancing heart–brain coupling research.

---

## 5. References

- Assenza, G., & Di Lazzaro, V. (2015). A useful electroencephalography (EEG) marker of brain plasticity: Delta waves. *Neural Regeneration Research*, 10(8), 1216. <https://doi.org/10.4103/1673-5374.162698>
- Benjamini, Y., & Hochberg, Y. (1995). Controlling the False Discovery Rate: A Practical and Powerful Approach to Multiple Testing. *Journal of the Royal Statistical Society, Series B*, 57(1), 289–300. <https://doi.org/10.1111/j.2517-6161.1995.tb02031.x>
- Bouhaddi, M., Vuillier, F., Fortrat, J. O., Cappelle, S., Henriet, M. T., Rumbach, L., & Regnard, J. (2004). Impaired cardiovascular autonomic control in newly and long-term-treated patients with Parkinson's disease: Involvement of l-dopa therapy. *Autonomic Neuroscience*, 116(1–2), 30–38. <https://doi.org/10.1016/j.autneu.2004.06.009>
- Bove, F., Mulas, D., Cavallieri, F., Castrioto, A., Chabardès, S., Meoni, S., Schmitt, E., Bichon, A., Di Stasio, E., Kistner, A., Pélissier, P., Chevrier, E., Seigneuret, E., Krack, P., Fraix, V., & Moro, E. (2021). Long-term Outcomes (15 Years) After Subthalamic Nucleus Deep Brain Stimulation in Patients With Parkinson Disease. *Neurology*, 97(3). <https://doi.org/10.1212/WNL.00000000000012246>
- Brener, J., & Ring, C. (2016). Towards a psychophysics of interoceptive processes: The measurement of heartbeat detection. *Philosophical Transactions of the Royal Society B: Biological Sciences*, 371(1708), 20160015. <https://doi.org/10.1098/rstb.2016.0015>
- Calne, D. B. (1970). Hypotension Caused by L-Dopa. *British Medical Journal*, 1, 474–475.
- Cambi, S., Solcà, M., Micali, N., & Berchio, C. (2024). Cardiac interoception in Anorexia Nervosa: A resting-state heartbeat-evoked potential study. *European Eating Disorders Review*, 32(3), 417–430. <https://doi.org/10.1002/erv.3049>
- Candia-Rivera, D., Catrambone, V., Barbieri, R., & Valenza, G. (2022). Functional assessment of bidirectional cortical and peripheral neural control on heartbeat dynamics: A brain-

---

heart study on thermal stress. *NeuroImage*, 251, 119023.

<https://doi.org/10.1016/j.neuroimage.2022.119023>

Candia-Rivera, D., Catrambone, V., Thayer, J. F., Gentili, C., & Valenza, G. (2022). Cardiac sympathetic-vagal activity initiates a functional brain–body response to emotional arousal. *Proceedings of the National Academy of Sciences*, 119(21), e2119599119.  
<https://doi.org/10.1073/pnas.2119599119>

Coll, M.-P., Hobson, H., Bird, G., & Murphy, J. (2021). Systematic review and meta-analysis of the relationship between the heartbeat-evoked potential and interoception. *Neuroscience & Biobehavioral Reviews*, 122, 190–200.  
<https://doi.org/10.1016/j.neubiorev.2020.12.012>

Critchley, H. D., & Harrison, N. A. (2013). Visceral Influences on Brain and Behavior. *Neuron*, 77(4), 624–638. <https://doi.org/10.1016/j.neuron.2013.02.008>

Dale, A., & Anderson, D. (1978). Information Variables in Voluntary Control and Classical Conditioning of Heart Rate: Field Dependence and Heart-Rate Perception. *Perceptual and Motor Skills*, 47(1), 79–85. <https://doi.org/10.2466/pms.1978.47.1.79>

Dirlich, G., Vogl, L., Plaschke, M., & Strian, F. (1997). Cardiac field effects on the EEG. *Electroencephalography and Clinical Neurophysiology*, 102(4), 307–315.  
[https://doi.org/10.1016/S0013-4694\(96\)96506-2](https://doi.org/10.1016/S0013-4694(96)96506-2)

Garfinkel, S. N., & Critchley, H. D. (2016). Threat and the Body: How the Heart Supports Fear Processing. *Trends in Cognitive Sciences*, 20(1), 34–46.  
<https://doi.org/10.1016/j.tics.2015.10.005>

Garrett, L., Trümbach, D., Spielmann, N., Wurst, W., Fuchs, H., Gailus-Durner, V., Hrabě De Angelis, M., & Höltner, S. M. (2023). A rationale for considering heart/brain axis control in neuropsychiatric disease. *Mammalian Genome*, 34(2), 331–350.  
<https://doi.org/10.1007/s00335-022-09974-9>

Gray, M. A., Taggart, P., Sutton, P. M., Groves, D., Holdright, D. R., Bradbury, D., Brull, D., & Critchley, H. D. (2007). A cortical potential reflecting cardiac function. *Proceedings*

---

of the National Academy of Sciences, 104(16), 6818–6823.

<https://doi.org/10.1073/pnas.0609509104>

Haapaniemi, T. H., Kallio, M. A., Korpelainen, J. T., Tolonen, U., Sotaniemi, K. A., Myllylä, V. V., & Suominen, K. (2000). Levodopa, bromocriptine and selegiline modify cardiovascular responses in Parkinson's disease. *Journal of Neurology*, 247(11), 868–874. <https://doi.org/10.1007/s004150070075>

Haslacher, D., Reber, P., Cavallo, A., Rosenthal, A., Pangratz, E., Beck, A., Romanczuk-Seiferth, N., Nikulin, V., Villringer, A., & Soekadar, S. R. (2025a). Heartbeat perception is causally linked to frontal delta oscillations. *Communications Biology*, 8(1), 1466. <https://doi.org/10.1038/s42003-025-08933-9>

Haslacher, D., Reber, P., Cavallo, A., Rosenthal, A., Pangratz, E., Beck, A., Romanczuk-Seiferth, N., Nikulin, V., Villringer, A., & Soekadar, S. R. (2025b). Heartbeat perception is causally linked to frontal delta oscillations. *Communications Biology*, 8(1), 1466. <https://doi.org/10.1038/s42003-025-08933-9>

Heimrich, K. G., Lehmann, T., Schlattmann, P., & Prell, T. (2021a). Heart Rate Variability Analyses in Parkinson's Disease: A Systematic Review and Meta-Analysis. *Brain Sciences*, 11(8), 959. <https://doi.org/10.3390/brainsci11080959>

Heimrich, K. G., Lehmann, T., Schlattmann, P., & Prell, T. (2021b). Heart Rate Variability Analyses in Parkinson's Disease: A Systematic Review and Meta-Analysis. *Brain Sciences*, 11(8), 959. <https://doi.org/10.3390/brainsci11080959>

Hünerli-Gündüz, D., Özbek İşbitiren, Y., Uzunlar, H., Çavuşoğlu, B., Çolakoğlu, B. D., Ada, E., Güntekin, B., & Yener, G. G. (2023). Reduced power and phase-locking values were accompanied by thalamus, putamen, and hippocampus atrophy in Parkinson's disease with mild cognitive impairment: An event-related oscillation study. *Neurobiology of Aging*, 121, 88–106. <https://doi.org/10.1016/j.neurobiolaging.2022.10.001>

Jammal Salameh, L., Bitzenhofer, S. H., Hanganu-Opatz, I. L., Dutschmann, M., & Egger, V. (2024). Blood pressure pulsations modulate central neuronal activity via

---

mechanosensitive ion channels. *Science*, 383(6682), eadk8511.  
<https://doi.org/10.1126/science.adk8511>

Kern, M., Aertsen, A., Schulze-Bonhage, A., & Ball, T. (2013). Heart cycle-related effects on event-related potentials, spectral power changes, and connectivity patterns in the human ECoG. *NeuroImage*, 81, 178–190. <https://doi.org/10.1016/j.neuroimage.2013.05.042>

Kim, K. J., Ramiro Diaz, J., Iddings, J. A., & Filosa, J. A. (2016). Vasculo-Neuronal Coupling: Retrograde Vascular Communication to Brain Neurons. *The Journal of Neuroscience*, 36(50), 12624–12639. <https://doi.org/10.1523/JNEUROSCI.1300-16.2016>

Knyazev, G. G. (2012). EEG delta oscillations as a correlate of basic homeostatic and motivational processes. *Neuroscience & Biobehavioral Reviews*, 36(1), 677–695. <https://doi.org/10.1016/j.neubiorev.2011.10.002>

Laborde, S., Mosley, E., & Thayer, J. F. (2017). Heart Rate Variability and Cardiac Vagal Tone in Psychophysiological Research – Recommendations for Experiment Planning, Data Analysis, and Data Reporting. *Frontiers in Psychology*, 08. <https://doi.org/10.3389/fpsyg.2017.00213>

Lachenmayer, M. L., Mürset, M., Antih, N., Debove, I., Muellner, J., Bompart, M., Schlaeppli, J.-A., Nowacki, A., You, H., Michelis, J. P., Dransart, A., Pollo, C., Deuschl, G., & Krack, P. (2021). Subthalamic and pallidal deep brain stimulation for Parkinson's disease—Meta-analysis of outcomes. *Npj Parkinson's Disease*, 7(1), 77. <https://doi.org/10.1038/s41531-021-00223-5>

Li, G., Jiang, S., Paraskevopoulou, S. E., Wang, M., Xu, Y., Wu, Z., Chen, L., Zhang, D., & Schalk, G. (2018). Optimal referencing for stereo-electroencephalographic (SEEG) recordings. *NeuroImage*, 183, 327–335. <https://doi.org/10.1016/j.neuroimage.2018.08.020>

Lischke, A., Pahnke, R., Mau-Moeller, A., & Weippert, M. (2021). Heart Rate Variability Modulates Interoceptive Accuracy. *Frontiers in Neuroscience*, 14, 612445. <https://doi.org/10.3389/fnins.2020.612445>

- 
- Malik, M. (1996). Heart Rate Variability: Standards of Measurement, Physiological Interpretation, and Clinical Use: Task Force of The European Society of Cardiology and the North American Society for Pacing and Electrophysiology. *Annals of Noninvasive Electrocardiology*, 1(2), 151–181. <https://doi.org/10.1111/j.1542-474X.1996.tb00275.x>
- Maris, E., & Oostenveld, R. (2007). Nonparametric statistical testing of EEG- and MEG-data. *Journal of Neuroscience Methods*.
- Marshall, A. C., Gentsch, A., Schröder, L., & Schütz-Bosbach, S. (2018). Cardiac interoceptive learning is modulated by emotional valence perceived from facial expressions. *Social Cognitive and Affective Neuroscience*, 13(7), 677–686. <https://doi.org/10.1093/scan/nsy042>
- Meng, L., Dunckley, E., & Xu, X. (2015). Effects of a single dose levodopa on heart rate variability in Parkinson’s disease. *Zhonghua Yi Xue Za Zhi*, 95(7), 493–495.
- Mouradian, M. M., Stoessl, A. J., & Lang, A. E. (2025). Disease-Modifying Trials in Treated Parkinson’s Disease: “Stable Treated” Does Not Equate with Biological Stability. *Movement Disorders*, 40(9), 1778–1790. <https://doi.org/10.1002/mds.30259>
- Müller, L. E., Schulz, A., Andermann, M., Gäbel, A., Gescher, D. M., Spohn, A., Herpertz, S. C., & Bertsch, K. (2015). Cortical Representation of Afferent Bodily Signals in Borderline Personality Disorder: Neural Correlates and Relationship to Emotional Dysregulation. *JAMA Psychiatry*, 72(11), 1077. <https://doi.org/10.1001/jamapsychiatry.2015.1252>
- Noack, C., Schroeder, C., Heusser, K., & Lipp, A. (2014). Cardiovascular effects of levodopa in Parkinson’s disease. *Parkinsonism & Related Disorders*, 20(8), 815–818. <https://doi.org/10.1016/j.parkreldis.2014.04.007>
- Oostenveld, R., Fries, P., Maris, E., & Schoffelen, J.-M. (2011). FieldTrip: Open Source Software for Advanced Analysis of MEG, EEG, and Invasive Electrophysiological

---

Data. *Computational Intelligence and Neuroscience*, 2011(1), 156869.

<https://doi.org/10.1155/2011/156869>

Owens, A. P., Friston, K. J., Low, D. A., Mathias, C. J., & Critchley, H. D. (2018). Investigating the relationship between cardiac interoception and autonomic cardiac control using a predictive coding framework. *Autonomic Neuroscience*, 210, 65–71.  
<https://doi.org/10.1016/j.autneu.2018.01.001>

Pang, J., Tang, X., Li, H., Hu, Q., Cui, H., Zhang, L., Li, W., Zhu, Z., Wang, J., & Li, C. (2019). Altered Interoceptive Processing in Generalized Anxiety Disorder—A Heartbeat-Evoked Potential Research. *Frontiers in Psychiatry*, 10, 616.  
<https://doi.org/10.3389/fpsyg.2019.00616>

Park, H.-D., & Blanke, O. (2019). Heartbeat-evoked cortical responses: Underlying mechanisms, functional roles, and methodological considerations. *NeuroImage*, 197, 502–511. <https://doi.org/10.1016/j.neuroimage.2019.04.081>

Park, H.-D., Blanke, O., Bernasconi, F., & Salomon, R. (2018). Neural Sources and Underlying Mechanisms of Neural Responses to Heartbeats, and their Role in Bodily Self-consciousness: An Intracranial EEG Study | Cerebral Cortex | Oxford Academic. *Cerebral Cortex*, 28, 2351–2364. <https://doi.org/10.1093/cercor/bhx136>

Park, H.-D., Correia, S., Ducorps, A., & Tallon-Baudry, C. (2014). Spontaneous fluctuations in neural responses to heartbeats predict visual detection. *Nature Neuroscience*, 17(4), 612–618. <https://doi.org/10.1038/nn.3671>

Patron, E., Mennella, R., Messerotti Benvenuti, S., & Thayer, J. F. (2019). The frontal cortex is a heart-brake: Reduction in delta oscillations is associated with heart rate deceleration. *NeuroImage*, 188, 403–410.

<https://doi.org/10.1016/j.neuroimage.2018.12.035>

Pollatos, O., & Schandry, R. (2004). Accuracy of heartbeat perception is reflected in the amplitude of the heartbeat-evoked brain potential. *Psychophysiology*, 41(3), 476–482.  
<https://doi.org/10.1111/1469-8986.2004.00170.x>

- 
- Poppa, T., Benschop, L., Horczak, P., Vanderhasselt, M.-A., Carrette, E., Bechara, A., Baeken, C., & Vonck, K. (2022). Auricular transcutaneous vagus nerve stimulation modulates the heart-evoked potential. *Brain Stimulation*, 15(1), 260–269. <https://doi.org/10.1016/j.brs.2021.12.004>
- Rinne, U. K., Birket-Smith, E., Dupont, E., Hansen, E., Hyppä, M., Marttila, R., Mikkelsen, B., Pakkenberg, H., & Presthus, J. (1975). Levodopa alone and in combination with a peripheral decarboxylase inhibitor benserazide (madopar®) in the treatment of Parkinson's disease: A controlled clinical trial. *Journal of Neurology*, 211(1), 1–9. <https://doi.org/10.1007/BF00312459>
- Sauseng, P., Klimesch, W., Gruber, W. R., Hanslmayr, S., Freunberger, R., & Doppelmayr, M. (2007). Are event-related potential components generated by phase resetting of brain oscillations? A critical discussion. *Neuroscience*, 146(4), 1435–1444. <https://doi.org/10.1016/j.neuroscience.2007.03.014>
- Schandry, R. (1981). Heart Beat Perception and Emotional Experience. *Psychophysiology*, 18(4), 483–488. <https://doi.org/10.1111/j.1469-8986.1981.tb02486.x>
- Schulz, A., Ferreira De Sá, D. S., Dierolf, A. M., Lutz, A., Van Dyck, Z., Vögele, C., & Schächinger, H. (2015). Short-term food deprivation increases amplitudes of heartbeat-evoked potentials. *Psychophysiology*, 52(5), 695–703. <https://doi.org/10.1111/psyp.12388>
- Schulz, A., Stammet, P., Dierolf, A. M., Vögele, C., Beyenburg, S., Werer, C., & Devaux, Y. (2018). Late heartbeat-evoked potentials are associated with survival after cardiac arrest. *Resuscitation*, 126, 7–13. <https://doi.org/10.1016/j.resuscitation.2018.02.009>
- Steinfath, P., Herzog, N., Fourcade, A., Sander, C., Nikulin, V., & Villringer, A. (2025). Validating genuine changes in heartbeat-evoked potentials using pseudotrials and surrogate procedures. *Imaging Neuroscience*, 3, IMAG.a.30. <https://doi.org/10.1162/IMAG.a.30>

- 
- Strohman, A., Isaac, G., Payne, B., Verdonk, C., Khalsa, S. S., & Legon, W. (2024). Low-intensity focused ultrasound to the insula differentially modulates the heartbeat-evoked potential: A proof-of-concept study. *Clinical Neurophysiology*, 167, 267–281. <https://doi.org/10.1016/j.clinph.2024.09.006>
- Tallon-Baudry, C., Bertrand, O., Delpuech, C., & Pernier, J. (1996). Stimulus Specificity of Phase-Locked and Non-Phase-Locked 40 Hz Visual Responses in Human. *The Journal of Neuroscience*, 16(13), 4240–4249. <https://doi.org/10.1523/JNEUROSCI.16-13-04240.1996>
- Tegegne, B. S., Man, T., Van Roon, A. M., Snieder, H., & Riese, H. (2020). Reference values of heart rate variability from 10-second resting electrocardiograms: The Lifelines Cohort Study. *European Journal of Preventive Cardiology*, 27(19), 2191–2194. <https://doi.org/10.1177/2047487319872567>
- Whitehead, W. E., Drescher, V. M., Heiman, P., & Blackwell, B. (1977). Relation of heart rate control to heartbeat perception. *Biofeedback and Self-Regulation*, 2(4), 371–392. <https://doi.org/10.1007/BF00998623>
- Whitsett, T. L., & Goldberg, L. I. (1972). Effects of Levodopa on Systolic Preejection Period, Blood Pressure, and Heart Rate during Acute and Chronic Treatment of Parkinson's Disease. *Circulation*, 45(1), 97–106. <https://doi.org/10.1161/01.CIR.45.1.97>
- Wolf, J.-P., Bouhaddi, M., Louisy, F., Mikehiev, A., Mourot, L., Cappelle, S., Vuillier, F., Andre, P., Rumbach, L., & Regnard, J. (2006). Side-effects of L-dopa on venous tone in Parkinson's disease: A leg-weighing assessment. *Clinical Science*, 110(3), 369–377. <https://doi.org/10.1042/CS20050247>
- Zeng, C., Zhang, M., Asico, L. D., Eisner, G. M., & Jose, P. A. (2007). The dopaminergic system in hypertension. *Clinical Science*, 112(12), 583–597. <https://doi.org/10.1042/CS20070018>

## 6. Appendix

Appendix 1 Table

Recording type	Patients (N)	EEG channels
Main	10	F3, F4, C3, C4, Cz, P3, P4, Pz
Supplementary	1	C3, C4, P3, P4
	1	F3, F4, C3, C4, P3, P4
	2	Fz, Cz, Oz, Pz, C3, C4

**Appendix 1 Overview of EEG channels.** Separated into the main and supplementary recording, this visualises the EEG channels available for the patients. There is a main overlap in central electrodes. This also explains the subsets chosen in this analysis.

Appendix 2 Table

Directionality	Channel 1	Channel 2
Ipsilateral	STN left	F3
	STN left	C3
	STN left	Pz
	STN right	F4
	STN right	C4
	STN right	Pz
Contralateral	STN left	F4
	STN left	C4
	STN right	F3
	STN right	C3

**Appendix 2 CCC channel combinations.** This table shows the combination and directionality of the chosen channels for the CCC.